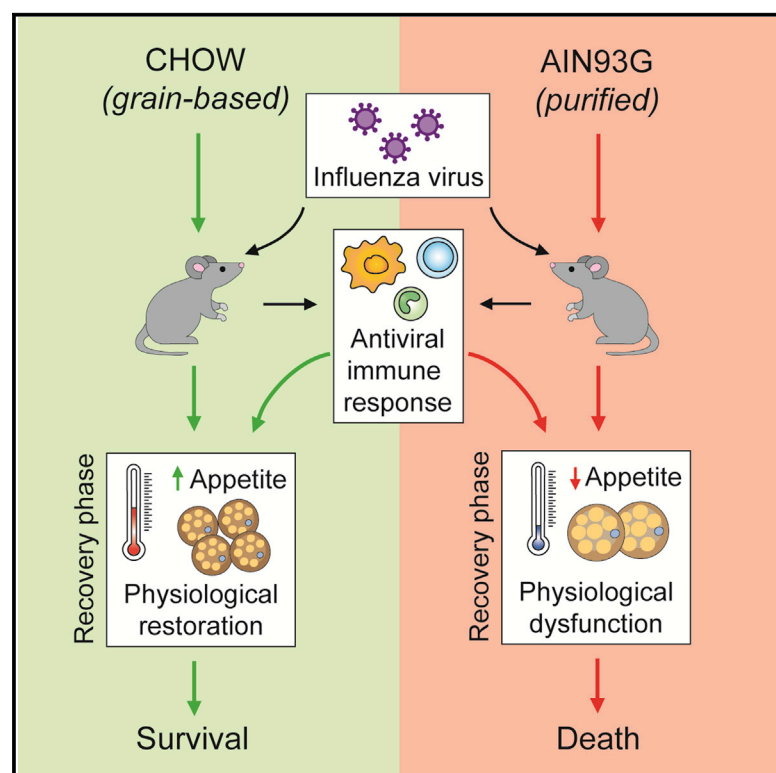


The quality of energy- and macronutrient-balanced diets regulates host susceptibility to influenza in mice

Graphical abstract



Authors

Taylor A. Cootes,
Nayan D. Bhattacharyya,
Susie S.Y. Huang, ..., Xinchun Chen,
Stephen J. Simpson, Carl G. Feng

Correspondence

carl.feng@sydney.edu.au

In brief

Cootes et al. show that diet formulation, independent of energy and macronutrient balance, regulates infection outcome and that highly processed foods are detrimental to host defense against influenza in mice. The study also highlights the importance of choosing adequate control diets in animal-based research.

Highlights

- Standard animal feeds show distinct abilities in supporting influenza-infected mice
- Mice on processed diet show increased mortality compared with those on grain-based feed
- Mice on processed diet fail to restore physiological homeostasis in infection
- Heightened susceptibility of processed-diet-fed mice is mediated by IFN- γ



Article

The quality of energy- and macronutrient-balanced diets regulates host susceptibility to influenza in mice

Taylor A. Cootes,^{1,2,3} Nayan D. Bhattacharyya,^{1,2,3} Susie S.Y. Huang,^{4,5} Lina Daniel,^{1,2,3} Kim S. Bell-Anderson,^{2,6} Sebastian A. Stifter,^{1,2,3} Tracy Chew,⁷ Samantha M. Solon-Biet,^{2,6} Luis R. Saraiva,^{4,8,9} Yi Cai,¹⁰ Xinchun Chen,¹⁰ Stephen J. Simpson,^{2,6} and Carl G. Feng^{1,2,3,11,12,*}

¹Immunology and Host Defense Group, School of Medical Sciences, Faculty of Medicine and Health, The University of Sydney, Sydney, NSW, Australia

²Charles Perkins Centre, The University of Sydney, Sydney, NSW, Australia

³Tuberculosis Research Program, Centenary Institute, The University of Sydney, Sydney, NSW, Australia

⁴Sidra Medicine, 26999 Doha, Qatar

⁵Division of Pediatric Cardiothoracic Surgery, Department of Surgery, Washington University School of Medicine, St. Louis, MO, USA

⁶School of Life and Environmental Sciences, Faculty of Science, The University of Sydney, Sydney, NSW, Australia

⁷Sydney Informatics Hub, Core Research Facilities, The University of Sydney, Sydney, NSW, Australia

⁸College of Health and Life Sciences, Hamad Bin Khalifa University, Doha, Qatar

⁹Monell Chemical Senses Center, 3500 Market Street, Philadelphia, PA 19104, USA

¹⁰Guangdong Key Laboratory of Regional Immunity and Diseases, Department of Pathogen Biology, Shenzhen University School of Medicine, Shenzhen, China

¹¹The University of Sydney Institute for Infectious Diseases, The University of Sydney, Sydney, NSW, Australia

¹²Lead contact

*Correspondence: carl.feng@sydney.edu.au

<https://doi.org/10.1016/j.celrep.2022.111638>

SUMMARY

Modulation of individual macronutrients or caloric density is known to regulate host resistance to infection in mice. However, the impact of diet composition, independent of macronutrient and energy content, on infection susceptibility is unclear. We show that two laboratory rodent diets, widely used as standard animal feeds and experimental controls, display distinct abilities in supporting mice during influenza infection. Mice placed on the highly processed AIN93G showed increased mortality to infection compared with those on a grain-based chow diet, suggesting a detrimental role for highly processed food in host defense. We further demonstrate that the heightened susceptibility of AIN93G-fed mice was associated with the failure in homeostasis restoration mediated by the cytokine interferon (IFN)- γ . Our findings show that diet composition calibrates host survival threshold by regulating adaptive homeostasis and highlights a pivotal role for extrinsic signals in host phenotype and outcome of host-pathogen interaction.

INTRODUCTION

Animal models for elucidating host defense mechanisms have traditionally focused on two interacting organisms: the pathogen and its host. However, it is now understood that environmental factors, such as diet, can also dictate host survival outcomes. While alterations of dietary macronutrients or caloric density are known to modulate infection susceptibility in mice,^{1–5} the impact of the dietary composition, independent of macronutrient and energy content, on infection outcome is unknown. We have previously demonstrated that the interaction between macronutrients, rather than calorie intake, regulates physiology^{6,7} and immune function⁸ in health, highlighting the importance of studying the composition of energy-balanced diets in infection.

Laboratory animal diets can be divided into two categories: grain-based and those containing purified ingredients. Although

both have equivalent protein, carbohydrate, and fat energy densities, grain-based and purified diets comprise of different ingredients, resulting in minor qualitative differences in the macro- and micronutrient content. For instance, grain-based diets typically obtain protein from soy instead of casein, thereby increasing the dietary phytoestrogen content.⁹ Furthermore, grain-based diets include whole-food ingredients, whereas purified diets are equivalent to ultra-processed foods (UPFs) in human food systems.¹⁰ There is growing evidence that UPFs are a major contributor to the global chronic disease burden,^{11,12} in part, due to their palatability and nutritional composition (low in nutrient density, low in fiber, and energy dense).¹³ There are also suggestions that the degree of processing per se is important.^{14,15} Whether the same applies to resistance to infectious diseases is an important, but unanswered, question.



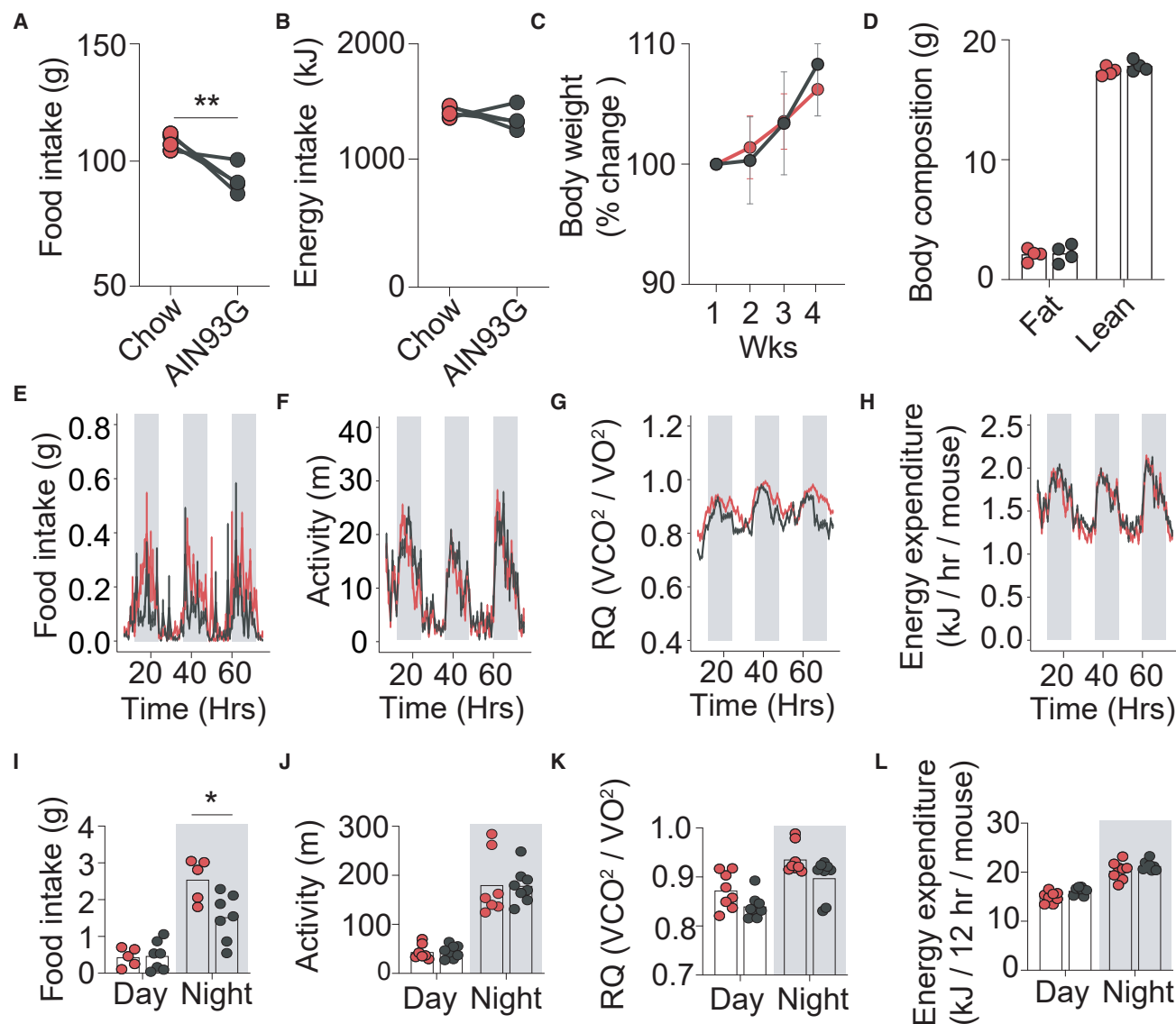


Figure 1. Energy-balanced chow and AIN93G diets show comparable ability in supporting the physiological health of naive mice

Naive WT mice were fed with chow (red symbols) or AIN93G (black symbols) diets *ad libitum* for 4 weeks, and food intake and energy metabolism were examined. (A and B) Food (A) and total energy (B) intake determined at 3 weeks. Symbols are group mean ($n = 5$ mice), and pair represents an individual experiment. Difference in food intake [(A) Student's t test $n = 4$, $t_6 = 4.72$, $p = 0.0033$].

(C) Change in body weight over 4 weeks of feeding (mean weight \pm SD, $n = 6$).

(D) Body composition measured using EchoMRI at 3 weeks.

(E–L) Three days prior to termination of the studies, some of the mice were transferred to metabolic cages, and food intake, RQ, activity, and energy expenditure of individually housed mice were monitored for 3 days. Data shown are group means ($n = 8$ mice) across 3 days (E–H) or individual animals ($n = 8$ mice) over 24 h (I–L).

In (D), and (I)–(L), each symbol represents an individual mouse and bars denote group mean. (I) Differences in food intake at night (Mann-Whitney test, $U = 5$, $p = 0.0480$). Data shown in (A)–(D) are representative of at least 3 experiments, and (E)–(L) are pooled from 2 independent experiments. * $p < 0.05$ and ** $p < 0.01$.

In this study, we report that grain-based (chow) and highly processed (AIN93G) diets, both known to support the growth of naive animals and used frequently as control diets in rodent studies, displayed distinct abilities in mediating resistance to influenza virus infection in mice, with AIN93G diet failing to support the survival of the infected hosts. Mechanistically, the heightened susceptibility is not due to impaired induction of anti-

viral immune response but to dysregulated adaptive homeostasis. Unexpectedly, the AIN93G diet-dependent lethality is mediated by virus-induced interferon (IFN)- γ . Together, these data demonstrate that subtle variations in dietary composition, including the extent of processing, are sufficient to alter host phenotype and disease severity. Therefore, this study establishes diet quality as a previously unappreciated determinant of

Table 1. The key macronutrients and energy contents of chow and AIN93G diets

Nutritional parameter ^a	Chow	AIN93G
Macronutrients (%)		
Protein	19	19.4
Total fat	4.6	7
Total digestible carbohydrate	59.90	56.8
Crude fiber	5.20	4.7
Acid detergent fiber	7.7	4.7
Neutral detergent fiber	15.50	
Energy contents		
Digestible energy (MJ/Kg)	14.2	16.1
Lipid-derived energy ^b	12	16
Protein-derived energy ^b	23	21

^aBased on the information provided by Specialty feeds (<https://www.specialtyfeeds.com/>).

^bThe percentage of total digestible energy.

host susceptibility to infection in mice, offering an additional mechanism to help explain the health impacts of ultra-processed diets in humans.

RESULTS

Commercial macronutrient- and energy-balanced diets show comparable ability in supporting the health of naive mice

To study the impact of diet quality on host defense against infection, we chose crude grain-based chow and highly processed AIN93G diets. Both diets are macronutrient and energy balanced and are commonly used in rodent studies as control diets. We first examined feeding behavior and multiple physiological parameters in naive wild-type (WT) C57BL6 female mice placed on either a chow or an AIN93G diet for 4 weeks. As reported previously,¹⁶ AIN93G-fed mice displayed decreased food consumption (Figure 1A) but similar energy intake (Figure 1B) compared with chow-fed animals due to the slightly higher energy content of AIN93G (Table 1). Consequently, chow- and AIN93G-fed mice showed comparable levels of weight gain (Figure 1C) as well as muscle and fat mass (Figure 1D).

To investigate the impact of dietary composition on respiratory and behavioral patterns under steady state, mice were housed individually in respirometry cages and monitored across 72 h. Consistent with our findings in Figure 1A, chow-fed mice displayed increased food consumption in night cycles (Figures 1E and 1I), while all animals showed comparable physical activity regardless of diet (Figures 1F and 1J). By measuring O₂ consumption and CO₂ output, we determined the respiratory quotient (RQ). Chow-fed mice displayed a trend toward a higher RQ than those on AIN93G (Figures 1G and 1K), indicating preferential oxidation of carbohydrates. Finally, we observed that mice on both diets exhibited comparable energy expenditure across a 72 h period during both day and night cycles (Figures 1H and 1L). Together, these findings confirm that chow and AIN93G diets are equally adequate in supporting the whole-body metabolism of naive mice.

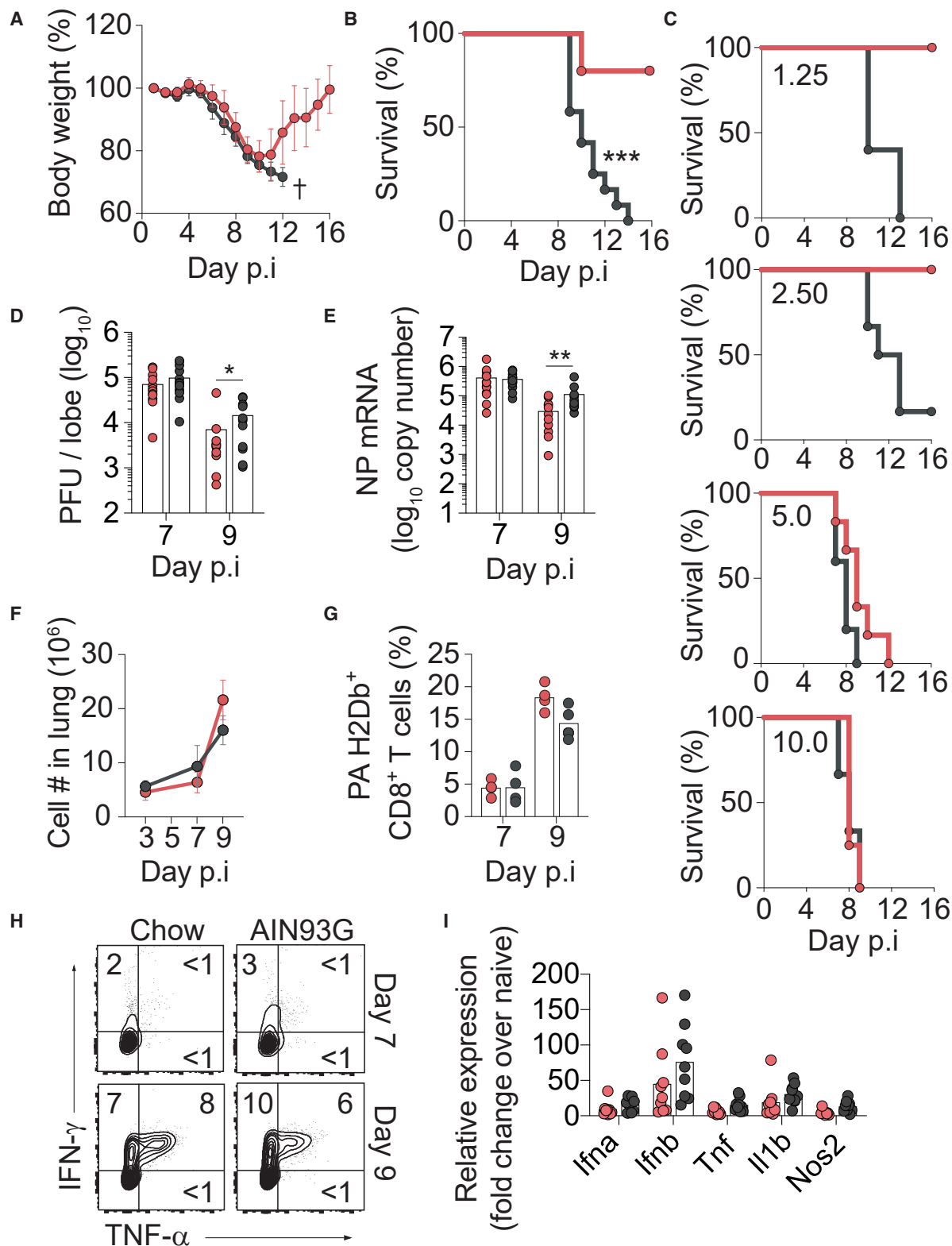
Chow- and AIN93G-fed mice show differential susceptibility to influenza infection

The ability of different rodent diets in supporting host defense against infection is unknown. Mice on chow or AIN93G for 3 weeks were inoculated intranasally (i.n.) with influenza A virus (IAV) and monitored for changes in body weight and survival. IAV infection triggered weight loss in both diet groups; however, while all chow-fed mice regained their weight after day 10 (Figure 2A), the mice on AIN93G failed to recover and subsequently succumbed to infection between days 12 and 14 (Figures 2A and 2B). To quantify the difference in the sensitivity of chow- and AIN93G-fed mice to IAV infection, graded doses of IAV were given to determine the lethal dose required to cause 50% mortality (LD50). The chow-fed mice exhibited an LD50 of 3.5 plaque-forming units (PFUs), almost triple that of the LD50 in the AIN93G-fed mice (1.2 PFUs; Figure 2C), indicating that AIN93G consumption increases the hosts' sensitivity to IAV infection.

We quantified the viral load (measured as PFU and viral nucleoprotein [NP] mRNA) in the lungs of day 7 and 9 infected mice. We observed that IAV loads of chow- and AIN93G-fed mice were comparable at day 7 and decreased in both groups by day 9 post infection (p.i.) (Figures 2D and 2E), suggesting containment of IAV infection regardless of diet type. To determine if the log-transformed PFU and NP means were statistically equivalent in the two diet groups, we performed Welch's two-sample equivalence t test. This analysis showed statistical evidence that PFU and NP levels were equivalent in the two diet groups at day 7 but not day 9, suggesting a possible delay in viral clearance in AIN93G-fed mice. However, analysis of host response in the lungs of chow- and AIN93G-fed mice did not reveal any difference in the extent of cell infiltration (Figure 2F), generation of IAV-specific (tetramer-positive) CD8⁺ T cells (Figure 2G), T cell effector function (Figure 2H), or expression of innate inflammatory genes (Figure 2I). These results suggest that mechanisms mediating the induction of immune response to IAV infection are not impaired in the AIN93G-fed mice.

AIN93G-fed mice fail to restore physiological homeostasis following infection

Maintaining physiological homeostasis and promoting tissue repair is critical in ensuring the survival of an infected host.^{17–19} However, the role of diet and its components in regulating host fitness remains poorly defined. To assess the physiological and metabolic parameters associated with host fitness in IAV infection, mice were individually housed in respirometry cages and continuously measured across 9 days of IAV infection. Like body weight (Figure 2A), the progression of IAV infection led to a gradual reduction in food intake, RQ, and energy expenditure in both chow- and AIN93G-fed mice (Figure 3). However, mice on the AIN93G diet consumed less food (Figures 3A and 3B) and recorded a lower RQ (Figure 3C) compared with chow-fed mice, which was most notable during the night cycle of the recovery phases (shown in boxed areas in Figures 3A and 3C) of IAV infection. The difference in food consumption between the two diet groups was greater in the infected than uninfected states (5.4- versus 1.5-fold difference; Figure 3B), suggesting that the small difference in caloric density between the two diets (Table 1) cannot fully account for the significant



(legend on next page)

reduction in food intake observed in the AIN93G-fed mice following infection. Nonetheless, the levels of energy expenditure were comparable between the two groups (Figure 3D), indicating that IAV infection leads to an energy deficit in the AIN93G-fed relative to chow-fed mice.

To investigate whether the increased mortality associated with persistent appetite loss is a result of food aversion or the physical and sensory properties of the diet, such as palatability, diet-swapping experiments were performed. Following 3 weeks of feeding on a given diet, mice were divided and placed on the other diet at day 0 or 7 of IAV infection. While replacing AIN93G with chow at day 0 protected the mice from IAV-induced death (Figure 3E, left panel), diet swapping on day 7 of infection (a time point before chow-fed mice begin to recover their appetite) failed to rescue the animals (Figure 3E, right). Interestingly, switching chow to AIN93G at day 7 also led to increased mortality, suggesting that the consumption of AIN93G during either early- or late-stage infection impairs host survival to influenza infection in mice. Importantly, these findings suggest that the persistent appetite loss in AIN93G-fed mice is not simply due to poor food palatability or conditioned taste aversion (CTA), where animals learn to associate a novel taste with illness and, as a consequence, avoid eating the food with this specific taste.²⁰

Since glucose utilization is required to fuel physiological programs and host survival to IAV infection,²¹ we assessed the impact of diet quality on glucose utilization before and after infection. While chow- and AIN93G-fed mice showed similar rate of glucose clearance under steady state, the latter animals exhibited slower glucose clearance than the former mice, indicating that AIN93G impairs glucose uptake in the infected host (Figure 3F). Finally, we observed that IAV-infected AIN93G-fed mice exhibited persistent and more severe core temperature loss compared with chow-fed mice (Figure 3G), suggesting that AIN93G is unable to restore temperature homeostasis in IAV-infected mice.

Chow and AIN93G diets induce distinct transcriptional responses in the hypothalamus and brown adipose tissue

To dissect the mechanisms underlying the perturbed physiological homeostasis in AIN93G-fed mice, we performed RNA sequencing (RNA-seq) analysis on the hypothalamus (Hypo), brown adipose

tissue (BAT), and liver from naive and IAV-infected mice fed on chow or AIN93G. Hierarchical clustering analysis of the 12 groups of mice showed that the gene-expression profiles clustered according to organ type and condition (Figure 4A). Next, we performed differential expression analysis on infected versus uninfected groups in the chow- and AIN93G-fed mice within each organ. When comparing infected with naive groups, the number of differentially expressed genes (DEGs) (\log_2 fold change [FC] > 1 and false discovery rate [FDR] < 0.05) in the BAT was higher in the AIN93G-fed mice than in the chow-fed mice (Figure 4B; Table S1). In contrast, the number of DEGs was comparable in the Hypo and liver of chow- and AIN93G-fed mice.

We next performed Gene Ontology (GO) enrichment analysis using the DEGs of the chow- and AIN93G-fed groups to identify potential diet-dependent biological processes. Analysis of the top 15 most significant pathways from each diet group revealed enrichment of immune-related pathways, driven mainly by IFNs, in all three organs regardless of diet regimen (Figure 4C; Table S2). However, fewer GO terms were shared between chow and AIN93G groups in the Hypo and BAT than in the liver.

GO enrichment analysis of DEGs in the Hypo of AIN93G-fed mice generated only 13 pathways compared with 40 in chow-fed mice (Table S2). All non-immune enriched pathways in the AIN93G-fed mice were negatively regulated by infection, including pathways related to DNA packaging (Figure 4C). In contrast, all enriched pathways in the Hypo of infected chow-fed mice were upregulated relative to their naive counterparts. The most prominently enriched non-immune pathways in IAV-infected chow-fed mice were associated with bone cell development. Distinct enrichment profiles between chow- and AIN93G-fed mice were also evident in the BAT. Specifically, pathways related to muscle cell development were preferentially enriched in the AIN93G-fed mice (Figure 4C). Together, these findings demonstrate that diet quality regulates transcriptional responses in organs critical for maintaining physiological and metabolic homeostasis during infection.

AIN93G diet alters cell differentiation programs in IAV-infected mice

Our finding that pathways associated with bone cell development were preferentially enriched in the Hypo of infected

Figure 2. Chow- and AIN93G-fed mice show differential susceptibility to influenza virus infection

Mice on chow (red) or AIN93G (black) diets for 3 weeks were inoculated with IAV (5 PFUs or otherwise indicated).

(A) Body weight change (mean weight \pm SD, $n = 10$).

(B) Difference in the survival of infected chow and AIN93G mice (log rank Mantel-Cox test, $n = 10$ –12, $\chi^2_1 = 14.67$, $p = 0.0001$).

(C) Survival of chow- and AIN93G-fed mice ($n = 5$) following infection with graded doses (indicated in the graphs) of IAV.

(D and E) PFU (D) and viral NP mRNA copy number (E) in the lungs at day 7 and 9 p.i. Statistical equivalence between diet groups were determined using Welch's two-sample equivalence t test. Equivalence boundaries were set based on the smallest standardized effect size of interest detectable at 90% power by t test ($n = 2$ –14, chow versus AIN93G, day 7, PFU $t_{21.83} = 2.295$, $p = 0.0159$, NP $t_{18.88} = 2.706$, $p = 0.00703$, and day 9, PFU $t_{18.9} = 1.647$, $p = 0.058$, NP, $t_{14.84} = 0.557$, $p = 0.293$).

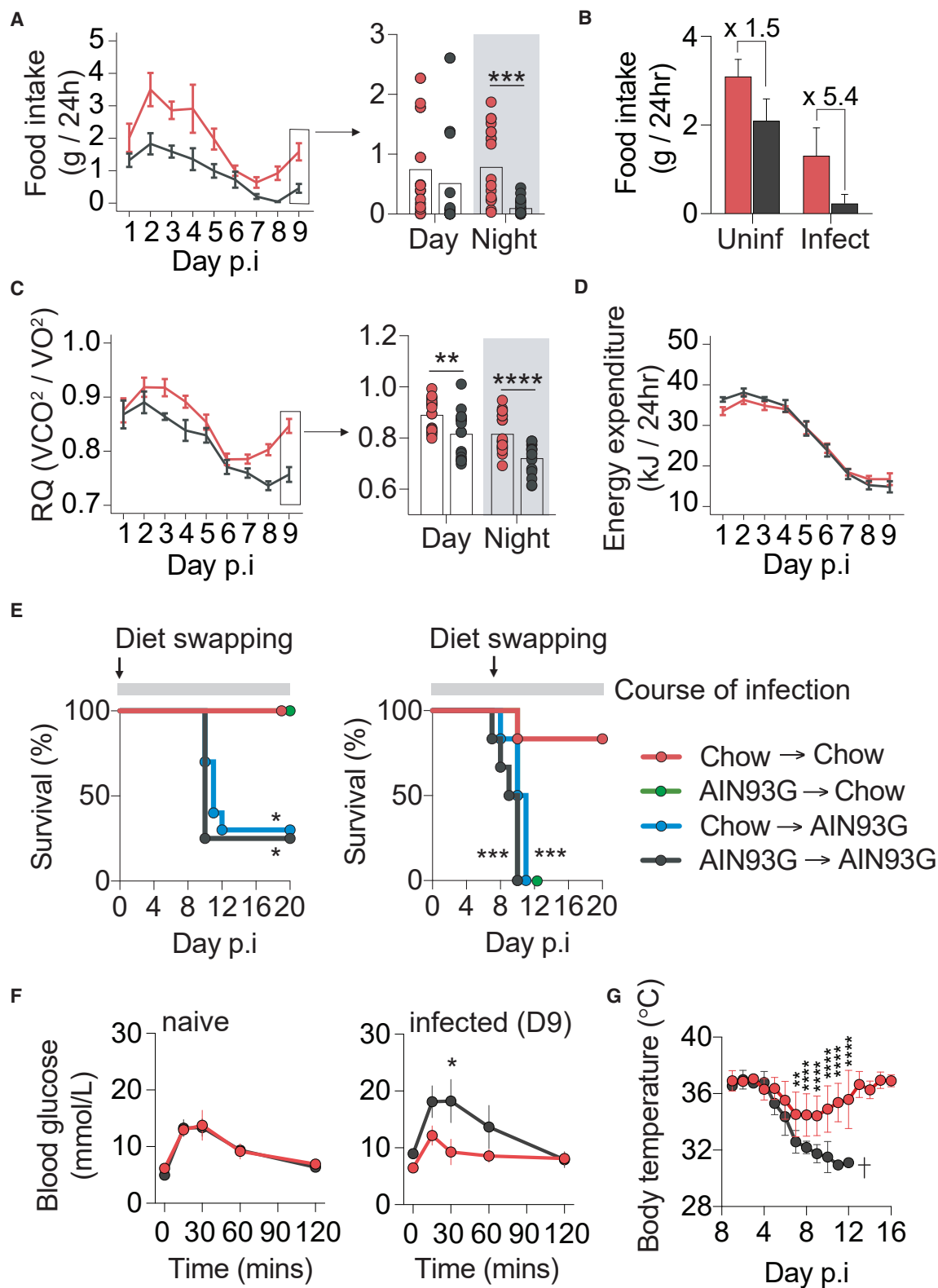
(F) Lung cell count (mean \pm SD, $n = 4$ –6) determined by trypan blue exclusion.

(G) Percentage of IAV-specific (PA-H2D^b) CD8⁺ T cells determined using flow cytometry after gating on pulmonary CD8⁺ T cells.

(H) Flow cytometric analysis of IFN- γ and TNF- α expression in CD44⁺CD8⁺ T cells.

(I) mRNA expression of innate inflammatory genes in the lungs of day 7 infected mice measured by qRT-PCR. Data shown are fold change relative to naive chow-fed mice.

In (D), (E), (G), and (I), symbols represent individual mice, and bars denote group mean. Data shown in (A) and (B) are representative of at least 5 independent experiments, in (D), (E), and (I) are pooled from 2–3 independent experiments and in (C) and (F)–(H) are representative of 2 experiments. * $p < 0.05$, ** $p < 0.01$, and *** $p < 0.001$.



(legend on next page)

chow-fed mice (Figure 4C) was unexpected. Further examination of the DEGs participating in these pathways revealed an abundance of genes encoding bone morphogenesis proteins (BMPs; members of the TGF- β superfamily) and related lipid mediators and transforming growth factor β (TGF- β) receptor components. In addition to bone morphogenesis, BMPs play an essential role in cell differentiation,²² tissue development,^{23,24} adipogenesis,^{25–27} and appetite.²⁸ We found that relative to their respective naive counterparts, the expression of *Bmp4*, *Bmp5*, *Bmp6*, and *Bmp7*, as well as *Lox* and *Tgfb3*, were significantly increased in the Hypo of the infected chow-fed, but not AIN93G-fed, mice (Figure 5A).

Brown adipocytes store more mitochondria than white adipocytes and express a set of unique thermoregulatory genes, including uncoupling protein-1 (*Ucp1*), which allows energy to be dissipated as heat without generating ATP. Brown adipocytes and myocytes are believed to share a common progenitor, mesenchymal stem cells.²⁹ Since pathways participating in muscle cell development were highly enriched in the BAT of the infected AIN93G-fed mice, we compared the expression of genes involved in adipogenesis and myogenesis between the two dietary groups in this tissue. Compared with infected chow-fed mice, myogenesis genes were upregulated while adipogenesis genes were downregulated in the infected AIN93G-fed mice (Figure 5B), suggesting that cell differentiation programs in BAT of chow- and AIN93G-fed mice are differentially regulated in IAV infection.

One of the markedly downregulated genes in the BAT of the infected AIN93G-fed mice is *Dio2*, known to be important for adaptive thermogenesis.³⁰ *Dio2* converts intracellular thyroxine (T4) to 3,5,3'-triiodothyronine (T3), thereby contributing to thermogenesis. To investigate whether impaired adipogenesis and *Dio2* expression contributes to the more severe hypothermia in the IAV-infected AIN93G-fed mice, we administered T3 daily to a subset of AIN93G-fed mice intraperitoneally (i.p.). Compared with their untreated counterparts, T3-treated, AIN93G-fed mice displayed significantly improved recovery from hypothermia (Figure 5C). These results indicate that the dysregulated thermogenesis could be a result of impaired T3 activity due to the reduced *Dio2* expression.

To determine whether chow and AIN93G diets differentially control the brown adipocyte response to IAV infection at the cellular and tissue levels, we quantified adipocyte number and size on H&E-stained BAT tissue sections at days 7 and 9 p.i. Based on eosin staining, brown adipocytes in the infected AIN93G-fed mice displayed lower mitochondrial content than that of the chow-fed animals, which was most apparent at day 7 after infection (Figure 5D). Moreover, compared with chow-fed mice, AIN93G-fed animals had significantly lower numbers of brown adipocytes, and these cells were larger in size at day 9 (Figure 5E). Finally, while the fat mass decreased in both chow and AIN93G groups at day 9 following infection, the reduction was more apparent in the AIN93G-fed animals (Figure 5F). Collectively, these data indicate that adipocytes in the BAT of chow- and AIN93G-fed animals undergo distinct transcriptomic and cellular changes in IAV infection, with the function of the latter group more severely impacted.

AIN93G-mediated susceptibility is dependent on virus-induced IFN- γ

Cytokines are common drivers of sickness-induced manifestations, including appetite loss³¹ and hypothermia.³² Since IFN- γ is one of the main cytokines produced in IAV infection and is known to trigger hypothermia in mice,³³ we examined the role of the cytokine in AIN93G-dependent disease susceptibility and observed that infected AIN93G-fed *Ifngr1*^{-/-}, but not WT, mice were able to regain their body weight and temperature to the same degree as chow-fed WT or *Ifngr1*^{-/-} mice (Figure 6A). Importantly, IFN- γ receptor signaling deficiency protected AIN93G-fed mice from lethality, suggesting that the impaired resilience of AIN93G-fed mice to IAV infection is mediated by IAV-induced IFN- γ .

We next determined whether AIN93G regulates local and systemic IFN- γ production. The *Ifng* gene was expressed at an extremely low level in the Hypo and BAT as shown by our RNA-seq analysis (data not shown). qRT-PCR analysis demonstrated that the *Ifng* mRNA was strongly induced in the lungs but not in other organs of chow- and AIN93G-fed animals (Figure 6B). Although T cells were readily detected in all organs analyzed (Figure S1A), IFN- γ -producing CD8⁺ and CD4⁺ T cells

Figure 3. Infected AIN93G-fed mice fail to restore physiological homeostasis

Mice were placed on different diets for 3 weeks and infected with 2.5 PFUs of IAV.

(A–D) Mice on chow (red) or AIN93G (black) were individually housed in metabolic cages and their physiological parameters monitored up to day 9 p.i.

(A) Food intake. Data shown are mean daily food intake over 9 days (left, n = 20) and individual intake over 24 h at day 9 (right). Differences between chow and AIN93G mice in food intake at night (right panel, U = 39, p < 0.0001).

(B) Fold differences in food intake between chow- and AIN93G-fed mice before and after infection (day 9) (n = 8–20).

(C) Changes in RQ. Data shown are mean daily RQ over 9 days (left, n = 18–20) and RQ of individual animal over 24 h at day 9 (right). Differences in RQ between diet groups (right panel, daytime, U = 92, p = 0.0091; night-time, U = 60, p = 0.0001).

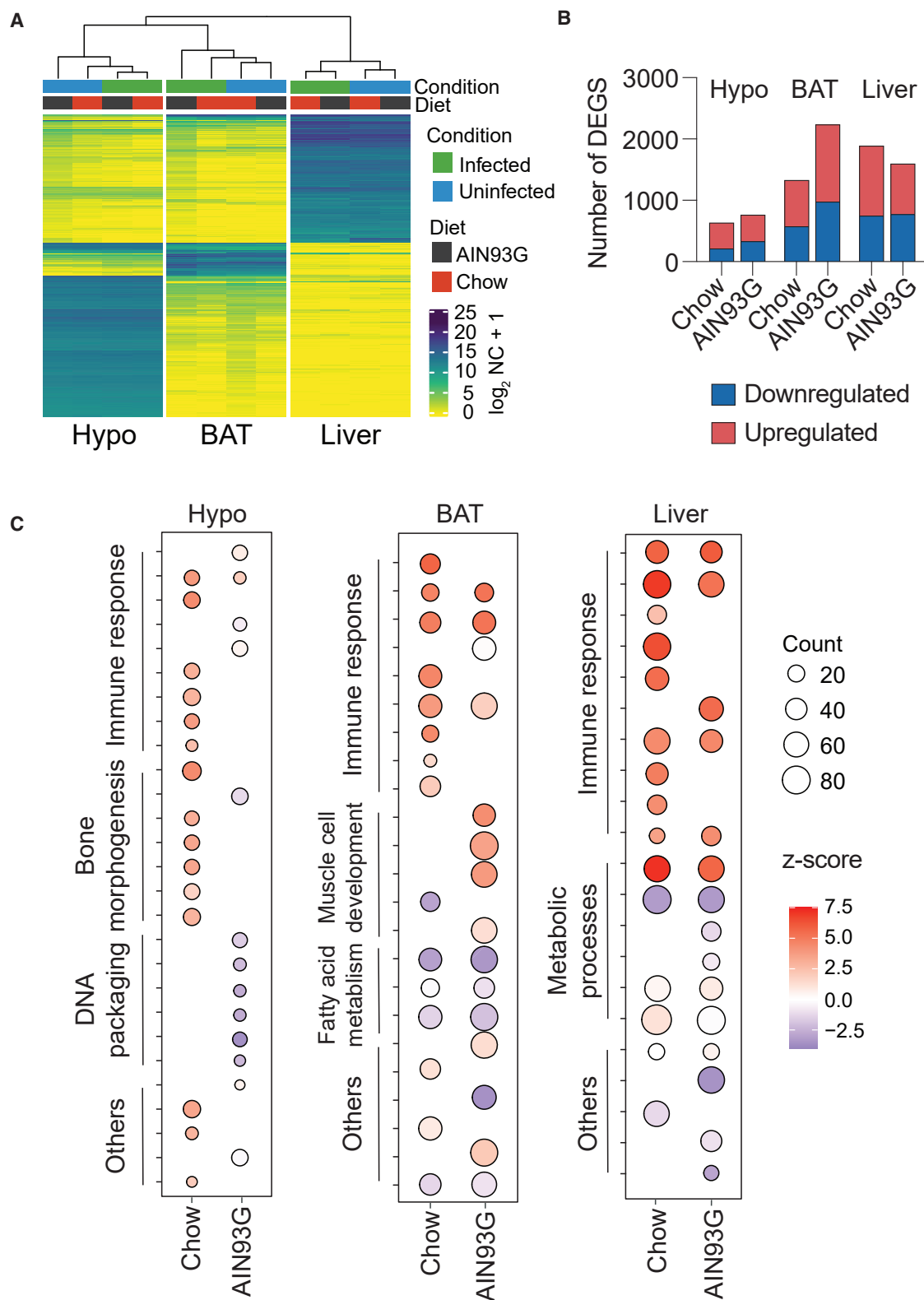
(D) Energy expenditure over 9 days following infection (n = 20).

(E) Survival of IAV-infected mice following diet swapping. Diets were swapped at either at day 0 (left panel, n = 6–10, $\chi^2_3 = 12.20$, p = 0.0067) or 7 (right panel, n = 6, $\chi^2_3 = 17.68$, p = 0.0005). Statistical significances shown are chow \rightarrow chow versus AIN93G \rightarrow chow, chow \rightarrow AIN93G, or AIN93G \rightarrow AIN93G mice.

(F) Difference in blood glucose in naive and day 9 infected chow and AIN93G mice following oral glucose administration (n = 5, diet effect in infected mice, $F_{1,6} = 15.54$, p = 0.0076).

(G) Difference in body temperature in infected chow- and AIN93G-fed mice after infection (n = 9, diet effect, $F_{1,1} = 25.11$, p = 0.0001). Body temperature was recorded daily using a rectal probe.

Data shown in (A) and (C), left panels, (B), (D), (F), and (G) are mean \pm SD. In (A) and (C), right panels, each symbol represents an individual mouse, and bars denote group mean. Data in (A)–(D) and (G) are pooled from 2 individual experiments and in (E) and (F) are representative of 2 experiments. Statistical analysis was performed using Mann-Whitney test (right panels in A and C), log rank Mantel-Cox test (E), two-way repeated-measures ANOVA (F), and mixed-effects analysis and Sidak multiple comparisons test (G). *p < 0.05, **p < 0.01, ***p < 0.001, and ****p < 0.0001.



(legend on next page)

were detected in the lung and liver (Figures S1B and S1C) but not the white adipose tissue (WAT) nor BAT (Figures S1D and S1E) of chow- and AIN93G-fed mice following *ex vivo* polyclonal restimulation. Although the *Ifng* level was higher in the lungs of the AIN93G-fed mice compared with chow-fed animals (Figure 6B), the percentage of cytokine-producing T cells in the same organ was comparable in both groups (Figures S1B and S1C), suggesting that other IFN- γ -producing cells, such as natural killer (NK) cells, may contribute to the increased *Ifng* mRNA expression in the lungs of AIN93G-fed mice. These findings indicate that, independently of diet used, IFN- γ is mainly produced in the infected lungs, which is consistent with the knowledge that active IAV infection is restricted to the epithelial cells of respiratory system. Therefore, the effect of IFN- γ on distant organs in IAV infection is likely mediated by circulating cytokine. We found that circulating IFN- γ was produced late during the infection (day 7) (Figure 6C), correlating with the divergence in homeostatic response between the diet groups. Circulating IFN- γ level was comparable in IAV-infected chow- and AIN93G-fed mice, confirming that the induction of IFN- γ and other antiviral responses (Figure 2) in our system is largely independent of the quality of diet and pointing to a role for AIN93G in regulating IFN- γ receptor signaling in infected mice.

We next determined the cell types mediating the detrimental effect of IFN- γ signaling in the AIN93G-fed mice by generating reciprocal bone marrow chimeras, in which either or both of the hematopoietic and stromal compartments were deficient in IFN- γ signaling. As expected, the absence of IFN- γ signaling in both the hematopoietic and stromal compartments led to reduced mortality (Figure 6D). Interestingly, IFN- γ signaling deficiency in either radio-sensitive or -resistant cells also resulted in partially enhanced survival, demonstrating that IFN- γ signaling is required in both hematopoietic and non-hematopoietic cells to impair the resilience of AIN93G-fed mice during IAV infection.

We next compared brown adipocyte number and size in AIN93G-fed WT and *Ifngr1*^{-/-} mice at day 9 p.i. As shown in Figure 5E, brown adipocytes in AIN93G-fed animals were lower in numbers and larger in size compared with those in chow-fed mice (Figure 6E). In contrast, the same measurements in AIN93G-fed *Ifngr1*^{-/-} mice were comparable with chow-fed WT mice. Interestingly, we found that thermogenesis genes were markedly downregulated in BAT of both diet groups following infection and that the downregulation was independent of IFN- γ signaling (Figure S2), suggesting that IFN- γ regulates some, but not all, metabolic programs in BAT.

We next investigated whether IFN- γ plays a role in regulating glucose metabolism in IAV-infected AIN93G-fed mice. Gluco-

neogenesis is critical for maintaining blood glucose levels during prolonged fasting, and pyruvate is believed to be the major substrate *in vivo*. i.p. injection of pyruvate (pyruvate tolerance test [PTT]) resulted in a more profound increase in blood glucose in infected mice than their naive counterparts (Figures S3A and S3B), suggesting an enhanced gluconeogenesis in IAV infection. AIN93G-fed WT mice, however, showed significantly delayed glucose clearance compared with their *Ifngr1*^{-/-} counterparts, which was mirrored in the glucose tolerance test (GTT). An insulin tolerance test (ITT) showed that infected WT mice were more resistant to insulin than *Ifngr1*^{-/-} mice, although the difference did not reach statistical significance. We speculate that IAV-induced IFN- γ impairs glucose uptake in infected AIN93G-fed mice possibly through modulating sensitivity of muscle cells to insulin signaling, a mechanism that has been demonstrated in a murine cytomegalovirus (MCMV) infection model.³⁴

To further understand how IFN- γ mediates the increased host susceptibility of AIN93G-fed mice in IAV infection, the possible role of nitric oxide was examined. Nitric oxide is highly induced by IFN- γ and is detrimental to host resistance to IAV infection in mice.^{35,36} We observed that treatment with the nitric oxide inhibitor L-NMMA improved recovery in body temperature and, to a lesser extent, body weight (Figure 6F) and reduced mortality rates (Figure 6G) in AIN93G-fed mice, demonstrating that the negative impact of IFN- γ on the survival of AIN93G-fed animals is at least partially dependent on nitric oxide. Together, the findings suggest that IFN- γ signaling modulates multiple mechanisms important in maintaining host physiological homeostasis in IAV-infected AIN93G-fed mice.

DISCUSSION

Infectious disease research in animals has predominately focused on host and pathogen interactions. Until recently, little consideration has been placed on the role of diet in the outcome of an infection. It is also assumed that all commercially available macronutrient- and energy-balanced diets are equally competent in supporting the survival of the infected host. Here, we demonstrate that diet formulation, independent of macronutrient balance and caloric intake, plays a previously unrecognized role in maintaining host fitness during influenza. These findings offer critical insight toward our understanding of how host physiological and immune systems, and ultimately the outcome of host-pathogen interactions, is regulated by diet.

Additionally, to the extent that chow versus purified diets in mice provide a model for comparing whole-food versus UPF diets in humans, our results provide another mechanism to explain

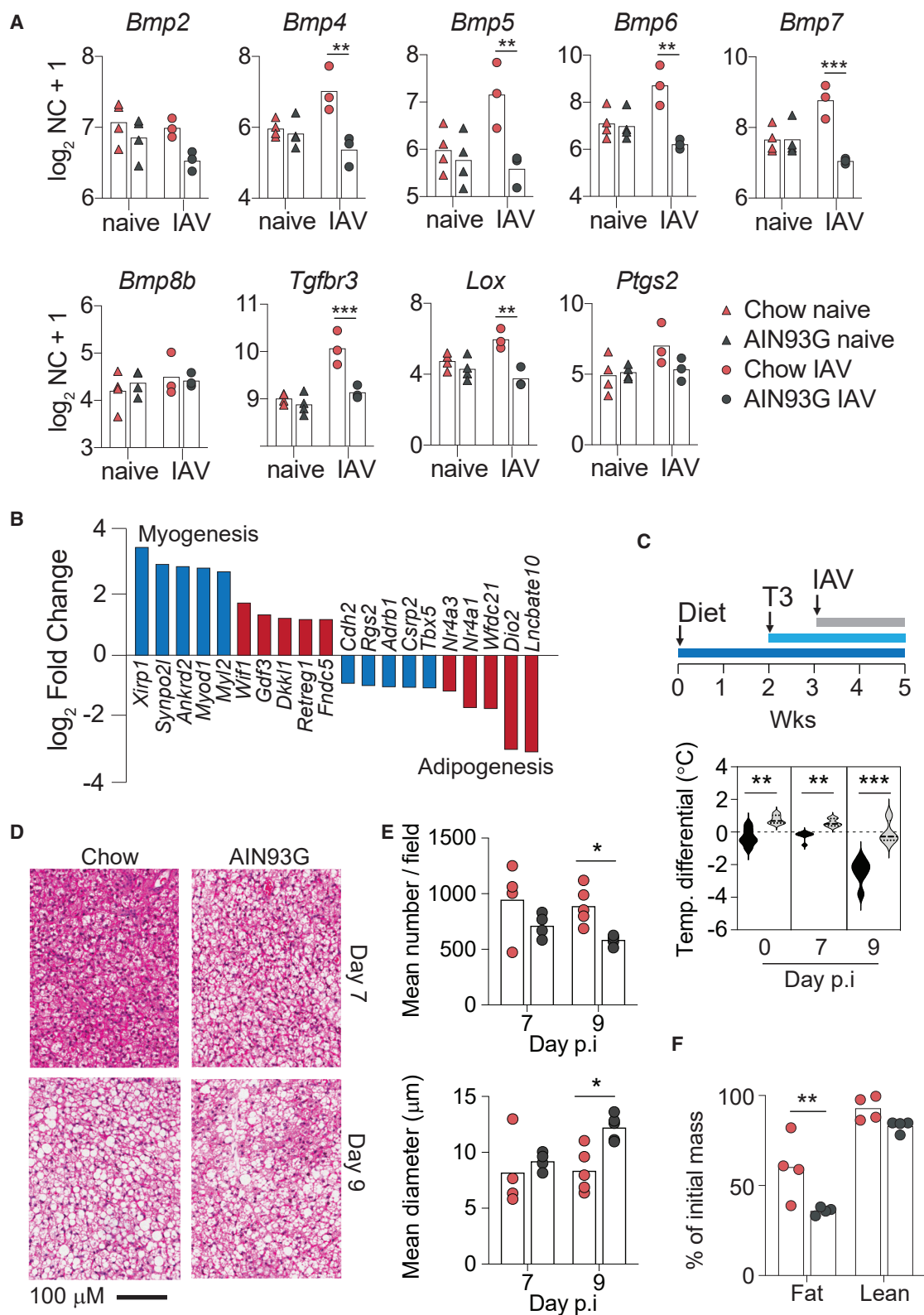
Figure 4. IAV-infected chow- and AIN93G-fed mice exhibit distinct transcriptomic landscapes in endocrinological and metabolic organs

Mice fed with chow or AIN93G were either left uninfected or infected with 5 PFU IAV. Hypothalamus (Hypo), brown adipose tissue (BAT), and liver were collected from uninfected or day 7 infected mice (n = 3–4) for RNA sequencing.

(A) Hierarchical clustering analysis of the top 500 most variable genes (rows) among 4 groups (columns) in the Hypo, BAT, and liver. mRNA expression levels are represented as mean normalized counts (NC) (n = 4) on a log₂(x+1) scale.

(B) Numbers of DEGs in Hypo, BAT, and liver of chow- or AIN93G-fed mice in infected versus uninfected analysis. DEGs were determined using a cutoff of FDR <0.05 and log₂FC of >1. Red and blue bars denote the numbers of up- and downregulated DEGs, respectively.

(C) GO enrichment analysis of DEGs from chow- and AIN93G-fed mice in infected versus uninfected analysis. Top 15 enriched pathways from each diet group are shown, except for AIN93G-fed mice in the Hypo with only 13 pathways enriched. Bubble size indicates the number of DEGs included in a pathway. Z score indicates up- (red) or downregulated (blue) pathways. Z score was calculated by subtracting the number of upregulated DEGs from the number of downregulated DEGs in a pathway from the GO enrichment analysis. This calculation was then divided by the square root of the total number of DEGs in a pathway.



(legend on next page)

the deleterious health impacts of UPFs in human food systems.^{10–12,15} Most emphasis to date has been placed on the role of UPFs in obesity and associated cardiometabolic diseases; our study brings to light how these diet-regulated physiological alterations can increase the susceptibility to infectious diseases.

In agreement with our findings, Milner et al. also noted a similar differential effect of chow and purified diets on the survival of IAV-infected mice.³ Our study reveals a regulatory role for diet quality in maintaining host physiological homeostasis. Sickness-induced anorexia and hypothermia have been suggested to be a defense mechanism that protects the host from tissue damage^{21,37,38} in some, but not all, infections. For instance, anorexia is protective in defense against bacterial infection but detrimental in viral and malarial infection.^{21,38} This study shows that the host-protective versus -detrimental function of these physiological mechanisms is further controlled by external factors, such as dietary formulation. Our findings therefore uncover a double-edged sword effect of disease-tolerance mechanisms, suggesting that sickness-induced manifestations must be tightly regulated.

Our findings reveal that IAV infection not only triggers significant immunological changes in the lung but also remodels the transcriptional landscape in the organs critical for energy metabolism (such as the Hypo, BAT, and liver). Importantly, we establish that the IAV-driven transcriptional signatures are regulated by diet composition. Diet has been identified as an extrinsic factor that can influence disease tolerance to infection in insects.^{39,40} Our findings show that nutrient composition plays a similar role in mammals. The significance of the enhanced expression of myogenesis genes in the BAT of AIN93G-fed mice relative to chow-fed mice is unclear. Brown adipocytes and skeletal muscle cells share an early development pathway and mechanisms that promote one differentiation process tend to repress alternative pathways.^{41,42} Therefore, enhanced myogenesis could be the cause or result of impaired adipogenesis. Alternatively, it could reflect an increase in a subset of adipocytes progressing through a myogenic intermediate state, a pro-

cess like that described in cold-induced beige adipocyte differentiation.⁴³

IFN- γ is identified as a mediator of AIN93G-diet-dependent susceptibility to IAV infection in this study. This cytokine is generally believed to play a minimal role in the survival of chow-fed C57BL6 mice infected with the PR8 strain of IAV.^{44–46} Therefore, the profound effect of IFN- γ on AIN93G-fed C57BL6 mice is unexpected. The host-detrimental function of IFN- γ is likely mediated by multiple mechanisms as we have shown that IFN- γ signals in both hematopoietic and non-hematopoietic compartments increase infection susceptibility. One possible mechanism of action is through the induction of nitric oxide, which is known to exacerbate influenza disease in mice.^{35,36} In addition, IFN- γ may also contribute to the glucose resistance observed in infected AIN93G-fed mice, a mechanism shown to operate in another viral infection model.³⁴

Our findings raise several questions regarding the design and approach of laboratory animal-based research. Should our investigation into the disease pathogenesis mechanisms in laboratory animals incorporate diet as a variable? Should mouse phenotype established using one diet be confirmed with another one, similar to the approach used to handle the genetic background issue with inbred laboratory mouse strains? Adequately addressing these questions may lead to changes in practice and, therefore, improvements in research reproducibility. Currently, grain-based and processed diets are used interchangeably in many nutrition and metabolism studies.^{47,48} For example, grain-based diets are incorrectly used as a control for high-fat or Western-style diets based on AIN93G formula. Finally, the findings from this investigation strongly support the notion that a multi-dimensional approach including immunology, physiology, microbiology, and nutrition is required to understand host-pathogen interactions.^{49,50}

Limitations of the study

Our study has several limitations. Firstly, the key diet component underlying differential survival outcome was not identified. While

Figure 5. Infected AIN93G-fed mice exhibit altered cell differentiation and tissue development in the Hypo and BAT

(A) Differential expression of BMP genes before (triangles) and after infection (circles) in the Hypo of chow (red) and AIN93G (black) mice ($n = 3–4$). *Bmp4* (diet effect, $F_{1,10} = 14.79$, $p = 0.0032$; infection status and diet interaction, $F_{1,10} = 10.60$, $p = 0.0086$); *Bmp5* (diet, $F_{1,10} = 9.78$, $p = 0.0107$; interaction, $F_{1,10} = 5.75$, $p = 0.0375$); *Bmp6* (diet, $F_{1,10} = 14.86$, $p = 0.0032$; interaction, $F_{1,10} = 12.51$, $p = 0.0054$); *Bmp7* (diet, $F_{1,10} = 16.54$, $p = 0.0023$; interaction, $F_{1,10} = 16.43$, $p = 0.0023$); *Tgfb3* (diet, $F_{1,10} = 14.79$, $p = 0.0052$; interaction, $F_{1,10} = 14.79$, $p = 0.0052$); and *Lox* (diet, $F_{1,10} = 20.12$, $p = 0.0012$; interaction, $F_{1,10} = 11.51$, $p = 0.0068$). Levels of mRNA expression are shown as NCs on a $\log_2(x+1)$ scale.

(B) Top 10 myogenesis and adipogenesis DEGs in the BAT of infected AIN93G-fed versus infected chow-fed mice. DEGs in analysis of infected AIN93G-fed versus infected chow-fed mice were determined by $FDR < 0.05$ and $\log_2FC > 1$. Blue and red bars denote genes involved in myogenesis and adipogenesis, respectively.

(C) Effect of T3 treatment in AIN93G-fed mice. Top, timelines of treatment. Some of the AIN93G-fed mice were injected daily i.p. with T3 starting 1 week prior to IAV infection. Bottom, difference in body temperature ($n = 6$, T3 treated versus untreated AIN93G-fed mice, $F_{1,10} = 84.78$, $p < 0.0001$; interaction, $F_{2,20} = 7.62$, $p = 0.0035$). Data shown are the differentials calculated by subtracting the body temperature of individual T3-treated (gray) and untreated (black) AIN93G-fed mice from the mean body temperature of chow-fed mice. Dotted line represents the temperature of the chow-fed mice at the respective time points.

(D) Representative images (40 \times) of H&E-stained BAT.

(E) Number (top) and diameter (bottom) of brown adipocytes at day 9 p.i. Differences between chow- (red) and AIN93G-fed (black) mice ($n = 4–5$) in cell number ($F_{1,14} = 9.20$, $p = 0.0090$) and diameter ($F_{1,14} = 6.78$, $p = 0.0209$). Symbol represents the mean value (for each mouse) of cell numbers or diameters quantified in four to five 300 \times 400 μ m fields of the tissue section.

(F) Change in fat and lean mass following IAV infection (fat mass difference, $n = 4$, $F_{1,12} = 12.50$, $p = 0.0041$). Data shown are the percentage of body mass of naive mice determined using EchoMRI.

In (A), (E), and (F), each symbol represents an individual mouse, and bars denote group mean. Data shown in (A) and (B) are from a single experiment, and (C)–(F) are representative of 2 independent experiments. Statistical analysis was performed using two-way ANOVA and Sidak's multiple comparisons test (A, E, and F) or two-way repeated measures ANOVA (C). * $p < 0.05$, ** $p < 0.01$, and *** $p < 0.001$.

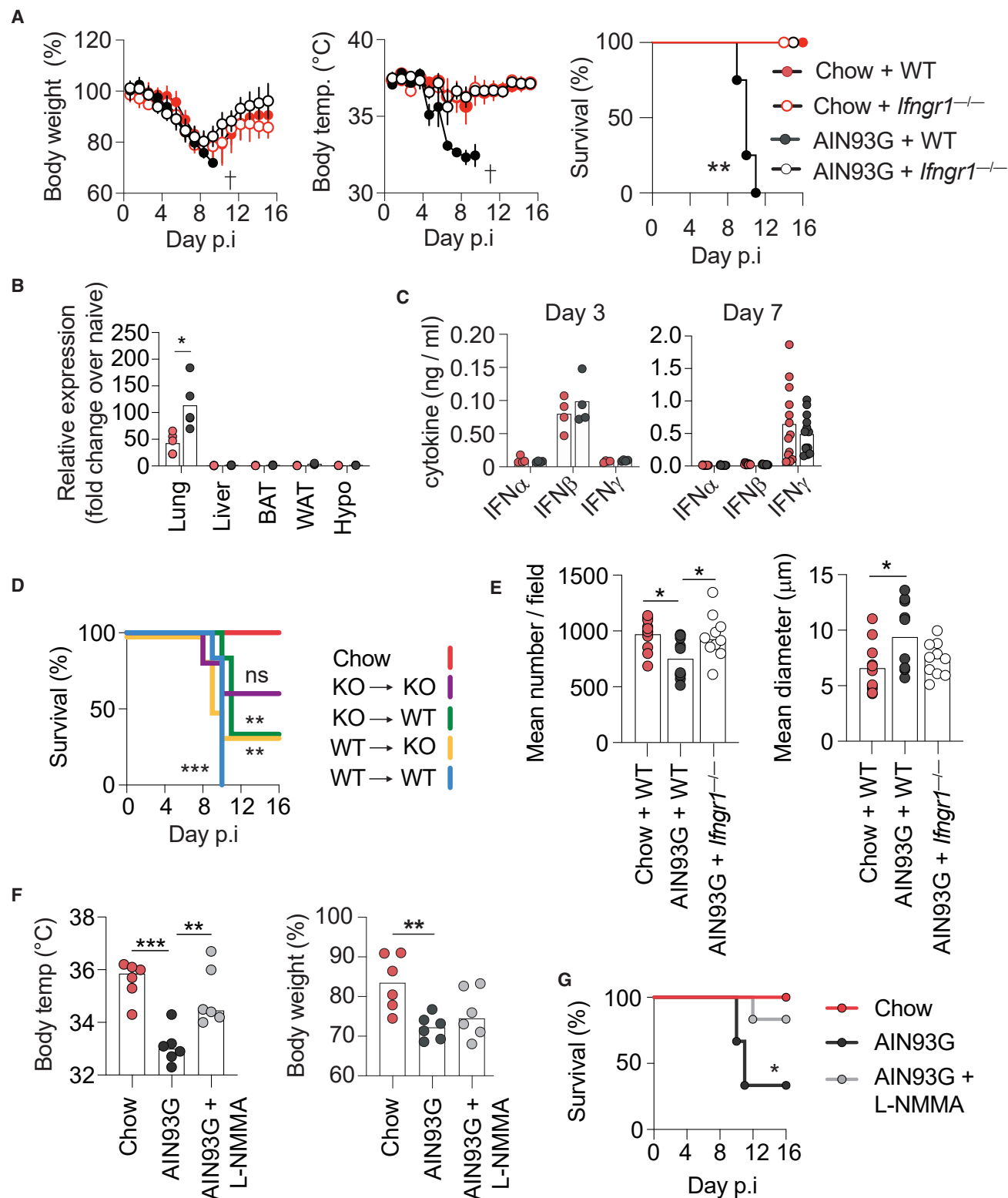


Figure 6. Increased susceptibility of AIN93G-fed mice to IAV infection is dependent on IFN- γ receptor signaling

WT and *Ifngr1*^{-/-} mice fed with chow or AIN93G for 3 weeks were infected with 5 PFU IAV.

(A) Body weight, temperature, and survival of infected WT and *Ifngr1*^{-/-} mice. Data shown are mean measurement \pm SD (left and middle panels, n = 4). Difference in the survival (right panel, n = 4, $\chi^2_3 = 20.75$, p = 0.0001). Statistical significances shown are AIN93G-fed WT versus AIN93G-fed *Ifngr1*^{-/-} mice.

(legend continued on next page)

the main difference between the two diets was related to the extent of processing or purification, multiple nutritional differences could have contributed to the impacts found. Unlike grain-based chow diets, which contain both soluble and insoluble fiber, AIN93G contains mainly cellulose, resulting in the absence of soluble fiber.⁵¹ Indeed, a role for fiber in defense against IAV infection in mice has been demonstrated.⁵ Similarly, difference in the fat content between the two diets could also influence the infection phenotype as a study performed in crickets has shown a trade-off between lipid transport and defense against infection.⁵² Secondly, the role of gut microbiome in the survival outcome was not investigated. Variations in diet processing or nutrient composition are known to control gut bacterial community diversity.^{7,8,53,54} Finally, only female C57BL6 mice were tested here. Recent studies have clearly demonstrated that sex and genetic background of animals regulate the metabolic response to dietary fat and protein.^{55,56} Whether diet quality impacts host defense against infection in male mice and/or mice on different genetic background remains to be determined. The interactions between diet, sex, and genetics may modulate host response to other types of stimuli beyond pathogens. In this regard, we have already shown that diet compositions can differentially regulate host response to several drugs.⁵⁷

STAR★METHODS

Detailed methods are provided in the online version of this paper and include the following:

- KEY RESOURCES TABLE
- RESOURCE AVAILABILITY
 - Lead contact
 - Materials availability
 - Data and code availability
- EXPERIMENTAL MODEL AND SUBJECT DETAILS
 - Mice
 - Rodent diets and feeding protocols
- METHOD DETAILS
 - Influenza A virus infection and mouse monitoring
 - Generation of bone marrow chimeric mice

- Treatments in mice
- Promethion cage study and EchoMRI
- Oral glucose tolerance, insulin tolerance and pyruvate tolerance test
- Preparation of single cell suspensions from lung
- Flow cytometry
- Histological analysis
- Cytokine quantification in plasma
- Viral plaque assays
- RNA preparation and qRT-PCR
- RNA sequencing

● QUANTIFICATION AND STATISTICAL ANALYSIS

SUPPLEMENTAL INFORMATION

Supplemental information can be found online at <https://doi.org/10.1016/j.celrep.2022.111638>.

ACKNOWLEDGMENTS

We thank Damien Chaussabel for his critical reading of this manuscript and helpful suggestions. We acknowledge Alex Shaw from the Sydney Informatics Hub for his excellent statistical consulting service and the University of Sydney's high-performance computing cluster, Artemis, for providing the computing resources that have contributed to the results reported herein. We acknowledge the Centenary Institute Animal and Flow Cytometry Core Facilities for their contributions to this work. We thank the NIH Tetramer Core Facility for providing the tetramer reagents. T.A.C., N.D.B., and L.D. are supported by an Australian Postgraduate Award. L.R.S. is funded by Sidra Medicine (SDR400078), a member of the Qatar Foundation.

AUTHOR CONTRIBUTIONS

Conceptualization, T.A.C., S.J.S., and C.G.F.; investigation, T.A.C., N.D.B., S.S.Y.H., L.D., K.S.B.-A., S.A.S., T.C., S.M.S.-B., and L.R.S.; writing – original draft, T.A.C. and C.G.F.; writing – review & editing, all authors; funding acquisition, C.G.F.; resources, Y.C. and X.C.; supervision, C.G.F.

DECLARATION OF INTERESTS

The authors declare no competing interests.

INCLUSION AND DIVERSITY

We support inclusive, diverse, and equitable conduct of research.

(B) *Irfn* mRNA expression as measured by qRT-PCR. Data shown are fold change relative to naive chow-fed mice (chow versus AIN93G in lung, $n = 4$, $t_8 = 3.19$, $p = 0.0128$).

(C) Levels of IFN proteins quantified in the plasma of chow- and AIN93G-fed mice at days 3 and 7 p.i.

(D) Survival of reciprocal bone marrow chimera. Lethally irradiated WT and *Irfn*^{1-/-} mice were reconstituted with WT or *Irfn*^{1-/-} bone marrow cells. Reconstituted mice were fed with AIN93G diet for 3 weeks before being infected with IAV. A group of infected chow-fed WT mice was included as a control. Statistical significances between chow and chimera groups are shown ($n = 12$, $\chi^2_4 = 29.74$, $p < 0.0001$). Statistical significance shown are chow group versus KO \rightarrow KO, KO \rightarrow WT, WT \rightarrow KO, or WT \rightarrow WT group.

(E) The number and dimension of adipocytes in WT and *Irfn*^{1-/-} mice at day 9 p.i. ($n = 5-6$, cell number, $F_{2,28} = 5.05$, $p = 0.0134$; dimension, $F_{2,28} = 3.94$, $p = 0.0312$). Symbol represents the mean value (for each mouse) of cell numbers or dimension quantified in four to five 300 \times 400 mm fields of the tissue section. (F and G) WT mice on chow or AIN93G were infected with IAV. Infected chow-fed mice were left untreated (red), whereas AIN93G-fed mice were either left untreated (black) or injected i.p. daily with L-NMMA (gray) starting on day 0.

(F) Body temperature (left) and weight (right) of L-NMMA-treated and untreated mice ($n = 5-6$). Body weight, $F_{2,15} = 6.28$, $p = 0.0105$. Body temperature, $F_{2,15} = 14.04$, $p = 0.0004$.

(G) Survival of L-NMMA-treated and untreated AIN93G mice ($n = 6-7$, $\chi^2_2 = 9.11$, $p = 0.0105$). Statistical significance in survival between treated and untreated AIN93G groups is shown.

In (B), (C), (E), and (F), each symbol represents an individual mouse, and bars denote group mean. Data shown in (A), (B), (F), and (G) are representative of 2 independent experiments and in (C)–(E) are pooled from 2–3 experiments. Statistical analysis was performed using log rank Mantel-Cox test (A, D, and G), Student's *t* test (B), and one-way ANOVA and Tukey's multiple comparisons test (E and F). * $p < 0.05$, ** $p < 0.01$, and *** $p < 0.001$.

Received: December 3, 2021
Revised: August 28, 2022
Accepted: October 19, 2022
Published: November 15, 2022

REFERENCES

- Gardner, E.M. (2005). Caloric restriction decreases survival of aged mice in response to primary influenza infection. *J. Gerontol. A Biol. Sci. Med. Sci.* 60, 688–694.
- Goldberg, E.L., Molony, R.D., Kudo, E., Sidorov, S., Kong, Y., Dixit, V.D., and Iwasaki, A. (2019). Ketogenic diet activates protective $\gamma\delta$ T cell responses against influenza virus infection. *Sci. Immunol.* 4, eaav2026.
- Milner, J.J., Rebeles, J., Dhungana, S., Stewart, D.A., Sumner, S.C.J., Meyers, M.H., Mancuso, P., and Beck, M.A. (2015). Obesity increases mortality and modulates the lung metabolome during pandemic H1N1 influenza virus infection in mice. *J. Immunol.* 194, 4846–4859.
- Taylor, A.K., Cao, W., Vora, K.P., De La Cruz, J., Shieh, W.J., Zaki, S.R., Katz, J.M., Sambhara, S., and Gangappa, S. (2013). Protein energy malnutrition decreases immunity and increases susceptibility to influenza infection in mice. *J. Infect. Dis.* 207, 501–510.
- Trompette, A., Gollwitzer, E.S., Pattaroni, C., Lopez-Mejia, I.C., Riva, E., Pernot, J., Ubags, N., Fajas, L., Nicod, L.P., and Marsland, B.J. (2018). Dietary fiber confers protection against Flu by shaping Ly6c(–) patrolling monocyte hematopoiesis and CD8(+) T cell metabolism. *Immunity* 48, 992–1005.e8.
- Solon-Biet, S.M., McMahon, A.C., Ballard, J.W.O., Ruohonen, K., Wu, L.E., Cogger, V.C., Warren, A., Huang, X., Pichaud, N., Melvin, R.G., et al. (2014). The ratio of macronutrients, not caloric intake, dictates cardiometabolic health, aging, and longevity in ad libitum-fed mice. *Cell Metab.* 19, 418–430.
- Solon-Biet, S.M., Mitchell, S.J., Coogan, S.C.P., Cogger, V.C., Gokarn, R., McMahon, A.C., Raubenheimer, D., de Cabo, R., Simpson, S.J., and Le Couteur, D.G. (2015). Dietary protein to carbohydrate ratio and caloric restriction: comparing metabolic outcomes in mice. *Cell Rep.* 11, 1529–1534.
- Le Couteur, D.G., Tay, S.S., Solon-Biet, S., Bertolino, P., McMahon, A.C., Cogger, V.C., Colakoglu, F., Warren, A., Holmes, A.J., Pichaud, N., et al. (2015). The influence of macronutrients on splanchnic and hepatic lymphocytes in aging mice. *J. Gerontol. A Biol. Sci. Med. Sci.* 70, 1499–1507.
- Brown, N.M., and Setchell, K.D. (2001). Animal models impacted by phytoestrogens in commercial chow: implications for pathways influenced by hormones. *Lab. Invest.* 81, 735–747.
- Monteiro, C.A., Cannon, G., Levy, R.B., Moubarac, J.C., Louzada, M.L., Rauber, F., Khandpur, N., Cediel, G., Neri, D., Martinez-Steele, E., et al. (2019). Ultra-processed foods: what they are and how to identify them. *Public Health Nutr.* 22, 936–941.
- Lauber, K., Rutter, H., and Gilmore, A.B. (2021). Big food and the World Health Organization: a qualitative study of industry attempts to influence global-level non-communicable disease policy. *BMJ Glob. Health* 6, e005216.
- Wells, J.C.K., Marfatia, A.A., Amable, G., Siervo, M., Friis, H., Miranda, J.J., Haisma, H.H., and Raubenheimer, D. (2021). The future of human malnutrition: rebalancing agency for better nutritional health. *Global Health* 17, 119.
- Martinez Steele, E., Raubenheimer, D., Simpson, S.J., Baraldi, L.G., and Monteiro, C.A. (2018). Ultra-processed foods, protein leverage and energy intake in the USA. *Public Health Nutr.* 21, 114–124.
- Hall, K.D., Ayuketah, A., Brychta, R., Cai, H., Cassimatis, T., Chen, K.Y., Chung, S.T., Costa, E., Courville, A., Darcey, V., et al. (2019). Ultra-processed diets cause excess calorie intake and weight gain: an inpatient randomized controlled trial of ad libitum food intake. *Cell Metab.* 30, 67–77.e3.
- Small, D.M., and DiFeliceantonio, A.G. (2019). Processed foods and food reward. *Science* 363, 346–347.
- Lang, P., Hasselwander, S., Li, H., and Xia, N. (2019). Effects of different diets used in diet-induced obesity models on insulin resistance and vascular dysfunction in C57BL/6 mice. *Sci. Rep.* 9, 19556.
- Ayres, J.S. (2020). The biology of physiological health. *Cell* 181, 250–269.
- Medzhitov, R., Schneider, D.S., and Soares, M.P. (2012). Disease tolerance as a defense strategy. *Science* 335, 936–941.
- Soares, M.P., Teixeira, L., and Moita, L.F. (2017). Disease tolerance and immunity in host protection against infection. *Nat. Rev. Immunol.* 17, 83–96. <https://doi.org/10.1038/nri.2016.136>.
- Chambers, K.C. (2018). Conditioned taste aversions. *World J. Otorhinolaryngol. Head Neck Surg.* 4, 92–100.
- Wang, A., Huen, S.C., Luan, H.H., Yu, S., Zhang, C., Gallezot, J.D., Booth, C.J., and Medzhitov, R. (2016). Opposing effects of fasting metabolism on tissue tolerance in bacterial and viral inflammation. *Cell* 166, 1512–1525.e12.
- Medici, D., Shore, E.M., Lounev, V.Y., Kaplan, F.S., Kalluri, R., and Olsen, B.R. (2010). Conversion of vascular endothelial cells into multipotent stem-like cells. *Nat. Med.* 16, 1400–1406.
- Sartori, R., Schirwis, E., Blaauw, B., Bortolanza, S., Zhao, J., Enzo, E., Stantzou, A., Mouisel, E., Toniolo, L., Ferry, A., et al. (2013). BMP signaling controls muscle mass. *Nat. Genet.* 45, 1309–1318.
- Hart, C.G., and Karimi-Abdolrezaee, S. (2020). Bone morphogenetic proteins: new insights into their roles and mechanisms in CNS development, pathology and repair. *Exp. Neurol.* 334, 113455.
- Schulz, T.J., Huang, P., Huang, T.L., Xue, R., McDougall, L.E., Townsend, K.L., Cypess, A.M., Mishina, Y., Gussoni, E., and Tseng, Y.H. (2013). Brown-fat paucity due to impaired BMP signalling induces compensatory browning of white fat. *Nature* 495, 379–383.
- Tseng, Y.H., Kokkotou, E., Schulz, T.J., Huang, T.L., Winnay, J.N., Taniguchi, C.M., Tran, T.T., Suzuki, R., Espinoza, D.O., Yamamoto, Y., et al. (2008). New role of bone morphogenetic protein 7 in brown adipogenesis and energy expenditure. *Nature* 454, 1000–1004.
- Blázquez-Medela, A.M., Jumabay, M., and Boström, K.I. (2019). Beyond the bone: bone morphogenetic protein signaling in adipose tissue. *Obes. Rev.* 20, 648–658.
- Townsend, K.L., Suzuki, R., Huang, T.L., Jing, E., Schulz, T.J., Lee, K., Taniguchi, C.M., Espinoza, D.O., McDougall, L.E., Zhang, H., et al. (2012). Bone morphogenetic protein 7 (BMP7) reverses obesity and regulates appetite through a central mTOR pathway. *FASEB J.* 26, 2187–2196.
- Kajimura, S., Seale, P., and Spiegelman, B.M. (2010). Transcriptional control of brown fat development. *Cell Metab.* 11, 257–262.
- de Jesus, L.A., Carvalho, S.D., Ribeiro, M.O., Schneider, M., Kim, S.W., Harney, J.W., Larsen, P.R., and Bianco, A.C. (2001). The type 2 iodothyronine deiodinase is essential for adaptive thermogenesis in brown adipose tissue. *J. Clin. Invest.* 108, 1379–1385.
- Rao, S., Schieber, A.M.P., O'Connor, C.P., Leblanc, M., Michel, D., and Ayres, J.S. (2017). Pathogen-mediated inhibition of anorexia promotes host survival and transmission. *Cell* 168, 503–516.e12.
- Schieber, A.M.P., and Ayres, J.S. (2016). Thermoregulation as a disease tolerance defense strategy. *Pathog. Dis.* 74, ftw106.
- Matthys, P., Dillen, C., Proost, P., Heremans, H., Van Damme, J., and Billaud, A. (1993). Modification of the anti-CD3-induced cytokine release syndrome by anti-interferon-gamma or anti-interleukin-6 antibody treatment: protective effects and biphasic changes in blood cytokine levels. *Eur. J. Immunol.* 23, 2209–2216.
- Šestan, M., Marinović, S., Kavazović, I., Cekinović, Đ., Wueest, S., Turk Wensveen, T., Brizić, I., Jonjić, S., Konrad, D., Wensveen, F.M., and Polić, B. (2018). Virus-induced interferon- γ causes insulin resistance in skeletal muscle and derails glycemic control in obesity. *Immunity* 49, 164–177.e6.

35. Akaike, T., Noguchi, Y., Ijiri, S., Setoguchi, K., Suga, M., Zheng, Y.M., Dietzschold, B., and Maeda, H. (1996). Pathogenesis of influenza virus-induced pneumonia: involvement of both nitric oxide and oxygen radicals. *Proc. Natl. Acad. Sci. USA* 93, 2448–2453.
36. Karupiah, G., Chen, J.H., Mahalingam, S., Nathan, C.F., and MacMicking, J.D. (1998). Rapid interferon gamma-dependent clearance of influenza A virus and protection from consolidating pneumonitis in nitric oxide synthase 2-deficient mice. *J. Exp. Med.* 188, 1541–1546.
37. Ganeshan, K., Nikkanen, J., Man, K., Leong, Y.A., Sogawa, Y., Maschek, J.A., Van Ry, T., Chagwedera, D.N., Cox, J.E., and Chawla, A. (2019). Energetic trade-offs and hypometabolic states promote disease tolerance. *Cell* 177, 399–413.e12.
38. Cumnock, K., Gupta, A.S., Lissner, M., Chevee, V., Davis, N.M., and Schneider, D.S. (2018). Host energy source is important for disease tolerance to malaria. *Curr. Biol.* 28, 1635–1642.e3.
39. Kutzer, M.A.M., and Armitage, S.A.O. (2016). The effect of diet and time after bacterial infection on fecundity, resistance, and tolerance in *Drosophila melanogaster*. *Ecol. Evol.* 6, 4229–4242.
40. Miller, C.V.L., and Cotter, S.C. (2018). Resistance and tolerance: the role of nutrients on pathogen dynamics and infection outcomes in an insect host. *J. Anim. Ecol.* 87, 500–510.
41. Harms, M., and Seale, P. (2013). Brown and beige fat: development, function and therapeutic potential. *Nat. Med.* 19, 1252–1263.
42. Seale, P., Bjork, B., Yang, W., Kajimura, S., Chin, S., Kuang, S., Scimè, A., Devarakonda, S., Conroe, H.M., Erdjument-Bromage, H., et al. (2008). PRDM16 controls a brown fat/skeletal muscle switch. *Nature* 454, 961–967.
43. Chen, Y., Ikeda, K., Yoneshiro, T., Scaramozza, A., Tajima, K., Wang, Q., Kim, K., Shinoda, K., Sponton, C.H., Brown, Z., et al. (2019). Thermal stress induces glycolytic beige fat formation via a myogenic state. *Nature* 565, 180–185.
44. Graham, M.B., Dalton, D.K., Giltinan, D., Braciale, V.L., Stewart, T.A., and Braciale, T.J. (1993). Response to influenza infection in mice with a targeted disruption in the interferon gamma gene. *J. Exp. Med.* 178, 1725–1732.
45. Nguyen, H.H., van Ginkel, F.W., Vu, H.L., Novak, M.J., McGhee, J.R., and Mestecky, J. (2000). Gamma interferon is not required for mucosal cytotoxic T-lymphocyte responses or heterosubtypic immunity to influenza A virus infection in mice. *J. Virol.* 74, 5495–5501.
46. Turner, S.J., Olivas, E., Gutierrez, A., Diaz, G., and Doherty, P.C. (2007). Disregulated influenza A virus-specific CD8⁺ T cell homeostasis in the absence of IFN-gamma signaling. *J. Immunol.* 178, 7616–7622.
47. Warden, C.H., and Fisler, J.S. (2008). Comparisons of diets used in animal models of high-fat feeding. *Cell Metab.* 7, 277.
48. Pellizzon, M.A., and Ricci, M.R. (2018). The common use of improper control diets in diet-induced metabolic disease research confounds data interpretation: the fiber factor. *Nutr. Metab.* 15, 3.
49. Ponton, F., Wilson, K., Cotter, S.C., Raubenheimer, D., and Simpson, S.J. (2011). Nutritional immunology: a multi-dimensional approach. *PLoS Pathog.* 7, e1002223.
50. Ponton, F., Wilson, K., Holmes, A.J., Cotter, S.C., Raubenheimer, D., and Simpson, S.J. (2013). Integrating nutrition and immunology: a new frontier. *J. Insect Physiol.* 59, 130–137.
51. Wise, A., and Gilbert, D.J. (1980). The variability of dietary fibre in laboratory animal diets and its relevance to the control of experimental conditions. *Food Cosmet. Toxicol.* 18, 643–648.
52. Adamo, S.A., Bartlett, A., Le, J., Spencer, N., and Sullivan, K. (2010). Illness-induced anorexia may reduce trade-offs between digestion and immune function. *Anim. Behav.* 79, 3–10.
53. Holmes, A.J., Chew, Y.V., Colakoglu, F., Cliff, J.B., Klaassens, E., Read, M.N., Solon-Biet, S.M., McMahon, A.C., Cogger, V.C., Ruohonen, K., et al. (2017). Diet-microbiome interactions in health are controlled by intestinal nitrogen source constraints. *Cell Metab.* 25, 140–151.
54. Solon-Biet, S.M., Walters, K.A., Simanainen, U.K., McMahon, A.C., Ruohonen, K., Ballard, J.W.O., Raubenheimer, D., Handelsman, D.J., Le Couteur, D.G., and Simpson, S.J. (2015). Macronutrient balance, reproductive function, and lifespan in aging mice. *Proc. Natl. Acad. Sci. USA* 112, 3481–3486.
55. Roy, S., Sleiman, M.B., Jha, P., Ingels, J.F., Chapman, C.J., McCarty, M.S., Ziebarth, J.D., Hook, M., Sun, A., Zhao, W., et al. (2021). Gene-by-environment modulation of lifespan and weight gain in the murine BXD family. *Nat. Metab.* 3, 1217–1227.
56. Green, C.L., Pak, H.H., Richardson, N.E., Flores, V., Yu, D., Tomasiewicz, J.L., Dumas, S.N., Kredell, K., Fan, J.W., Kirsh, C., et al. (2022). Sex and genetic background define the metabolic, physiologic, and molecular response to protein restriction. *Cell Metab.* 34, 209–226.e5.
57. Le Couteur, D.G., Solon-Biet, S.M., Parker, B.L., Pulpitel, T., Brandon, A.E., Hunt, N.J., Wali, J.A., Gokam, R., Senior, A.M., Cooney, G.J., et al. (2021). Nutritional reprogramming of mouse liver proteome is dampened by metformin, resveratrol, and rapamycin. *Cell Metab.* 33, 2367–2379.e4.
58. Randhawa, M.A. (2009). Calculation of LD50 values from the method of miller and tainter, 1944. *J. Ayub Med. Coll. Abbottabad* 21, 184–185.
59. Stifter, S.A., Bhattacharyya, N., Sawyer, A.J., Coates, T.A., Stambas, J., Doyle, S.E., Feigenbaum, L., Paul, W.E., Britton, W.J., Sher, A., and Feng, C.G. (2019). Visualizing the selectivity and dynamics of interferon signaling in vivo. *Cell Rep.* 29, 3539–3550.e4.
60. Bhattacharyya, N.D., Counoupas, C., Daniel, L., Zhang, G., Cook, S.J., Coates, T.A., Stifter, S.A., Bowen, D.G., Triccas, J.A., Bertolino, P., et al. (2021). TCR affinity controls the dynamics but not the functional specification of the antimycobacterial CD4. *J. Immunol.* 206, 2875–2887. <https://doi.org/10.4049/jimmunol.2001271>.
61. Huang, S.S.Y., Makhlof, M., AbouMoussa, E.H., Ruiz Tejada Segura, M.L., Mathew, L.S., Wang, K., Leung, M.C., Chaussabel, D., Logan, D.W., Scialdone, A., et al. (2020). Differential regulation of the immune system in a brain-liver-fats organ network during short-term fasting. *Mol. Metab.* 40, 101038.

STAR★METHODS

KEY RESOURCES TABLE

REAGENT or RESOURCE	SOURCE	IDENTIFIER
Antibodies		
Fc Block (2.4G2)	BD	553142; RRID: AB_394657
CD4 - AF700 (RM4-5)	BD	557956; RRID: AB_396956
CD8 - BV711 (53-6.7)	BD	563046; RRID: AB_2737972
CD44 - BV605 (IM7)	BD	563058; RRID: AB_2737979
IFN- γ - PE/Cy7 (XMG1.2)	BD	561040; RRID: AB_396766
TNF- α - PerCP/Cy5.5 (MP6-XT22)	BioLegend	506321; RRID: AB_961435
PE-conjugated PA ₂₂₄₋₂₃₃ :H2-D ^b tetramer	NIH	N/A
Purified NA/LE Anti-CD3e (145-2C11)	BD	553057; RRID: AB_394590
Bacterial and virus strains		
PR8: A/PR/8/34 (H1N1)	Common passaged lab strain - grown in house	N/A
Chemicals, peptides, and recombinant proteins		
UV Live/Dead	Thermo Fisher	Cat# L34962
RNAlater	Sigma Aldrich	Cat# R0901-500ML
Trisure	Bioline	Cat# BIO-38033
DNase I	Sigma Aldrich	Cat# DN25-100MG; Cas: 9003-98-9
L-NMMA	Cayman Chemical	10005031 ; RRID: 53308-83-1
L-15 Media	Sigma Aldrich	Cat# L4386-10X1L
Avicel	Sigma Aldrich	11365; Cas: 9004-34-6
Glucose	Sigma Aldrich	G8270-100G; Cas: 50-99-7
Insulin (Actrapid)	ThePharmacy	NA
Pyruvate	Sigma Aldrich	P2256; Cas: 113-24-6
EDTA	Thermo Fisher	Cat# 15575020
T3 (3,3',5'-Triiodo-L-thyronine)	Cayman Chemical	17598; Cas: 5817-39-0
Trypsin	Worthington Biochemicals	Cat# LS003740
Collagenase type IV	Sigma Aldrich	C5138; Cas: 9001-12-1
Collagenase type II	Sigma Aldrich	C6885; Cas: 9001-12-1
Fixation/Permeabilization Kit	BD	554714; RRID: AB_2869008
Critical commercial assays		
LegendPlex Mouse Type I/II IFN Panel	BioLegend	Cat# 740635
Tetro cDNA synthesis Kit	Bioline	Cat# BIO-65043
SYBR No-ROX Master Mix	Bioline	Cat# BIO-98020
Deposited data		
RNAseq data	This paper	GEO: GSE215976
Experimental models: Cell lines		
MDCK	Common cell line – grown in house	N/A
Experimental models: Organisms/strains		
C57BL/6J	Australian BioResources	N/A
<i>Ifngr</i> ^{1-/-} (B6.129S7- <i>Ifngr</i> ^{tm1Agt/J})	The Jackson Laboratory	003288
Oligonucleotides		
See Table S3 for oligonucleotide sequences	N/A	N/A
Software and algorithms		
GraphPad Prism 8	GraphPad Software	RRID: SCR_002798
MetaScreen	Sable Systems	https://www.sablesys.com

(Continued on next page)

Continued

REAGENT or RESOURCE	SOURCE	IDENTIFIER
ImageScope	Leica Biosystems	https://www.leicabiosystems.com
RStudio	RStudio	https://www.rstudio.com
FACSDiva Software	BD	https://www.bdbiosciences.com
FlowJo10	TreeStar	https://www.flowjo.com
QuPath	Queen's University	https://qupath.github.io
Other		
Irradiated chow diet (Meat Free Rat and Mouse Diet)	Specialty Feeds	https://www.specialtyfeeds.com/new/wp-content/uploads/2016/06/irr_rm.pdf
Irradiated AIN93G diet + extra vitamins	Specialty Feeds	SF09-091
Promethion behavioral phenotyping cages	Sable Systems	Multiple
Rectal thermometer	Physitemp Instruments	N/A
Leica Aperio XT slide scanner	Leica Biosystems	https://www.leicabiosystems.com
Roche LightCycler480	Roche	https://diagnostics.roche.com
NanoDrop 2000c	Thermo Fisher Scientific	Cat# ND-2000
Illumina HiSeq 2000	Illumina	https://www.illumina.com
BD Fortessa	BD	https://www.bdbiosciences.com
EchoMRI-900	EchoMRI LCC	http://www.echomri.com
Glucometer	Abbott	N/A

RESOURCE AVAILABILITY

Lead contact

Further information and requests for resources and reagents should be directed to and will be fulfilled by the lead contact, Carl Feng (carl.feng@sydney.edu.au).

Materials availability

This study did not generate new unique reagents.

Data and code availability

RNA-seq data has been deposited at GEO and is publicly available as of the date of publication. Accession numbers are listed in the [key resources table](#). This paper does not report original code. Any additional information required to reanalyze the data reported in this paper is available from the [lead contact](#) upon request.

EXPERIMENTAL MODEL AND SUBJECT DETAILS

Mice

Mice were maintained under specific pathogen-free conditions at University of Sydney Charles Perkins Centre and Centenary Institute with the ethics approvals from the University of Sydney (protocol 2019-066) and Sydney Local Health District (2015-037 and 2020-007), respectively. Wild-type (WT) C57BL/6 mice were purchased from Australian BioResources (Moss Vale, NSW, Australia). *Ifngr1*^{-/-} mice on C57BL/6 background were bred in the Centenary Institute. Female animals aged between 6 and 20 wk old were used for all experiments. Mice were provided food and water *ad libitum* and housed in a temperature and humidity-controlled environment with a 12-hour light and 12-hour dark cycle.

Rodent diets and feeding protocols

Irradiated chow diet (Meat Free Rat and Mouse Diet) and a AIN93G diet supplemented with extra vitamins (SF09-091) were purchased from Specialty Feeds (Glen Forrest, Western Australia). Unless specified, mice were pre-conditioned with chow or AIN93G diet for 3w before exposing to influenza virus.

For diet swapping experiments, mice were first fed on their condition diet (chow or AIN93G) for 3w and then switched to the alternative diet at either day 0 or day 7 p.i.. Some mice were maintained on chow and AIN93G throughout the studies as controls.

METHOD DETAILS

Influenza A virus infection and mouse monitoring

After anaesthetizing with ketamine and xylazine, mice were inoculated intranasally with 2.5 or 5 PFU of mouse-adapted influenza A virus (strain A/Puerto Rico/8/1934 H1N1, kindly provided by Dr John Stambas) in 40 μ L of sterile PBS. For the majority of metabolic and immunological analysis experiments, a lower inoculant dose 2.5 PFU was used. Viral dose required for 50% of the lethality (LD50) was calculated as previously described method.⁵⁸ Mice were scored and monitored daily for food intake, body weight and temperature throughout the course of the study. Food consumption per cage was monitored by weighing food in the hopper. Body temperature of individual animals were recorded using a rectal thermometer.

Generation of bone marrow chimeric mice

Lethally irradiated (10 Gy) naïve WT C57BL6 and *Ifngr1*^{-/-} recipient mice were reconstituted with 2×10^6 bone marrow cells from *Ifngr1*^{-/-} or C57BL6 mice by tail vein injection. Mice were maintained on antibiotic (Trimethoprim sulpha)-supplemented drinking water for 4 wk after irradiation. Mice were used for infection experiments after at least 8 wk when the recipient mice were fully reconstituted.

Treatments in mice

For nitric oxide inhibition *in vivo*, L-NMMA (Cayman Chemical) was administered i.p. daily (2 mg/kg in PBS) until mice recovered or reached their humane endpoint. T3 (3,3',5-Triiodo-L-thyronine) (Cayman Chemical) treatment was initiated 7 days before IAV infection and continued throughout the duration of the study. T3 (100 μ g/kg in PBS) was administered daily by i.p. injection.

Promethion cage study and EchoMRI

Mice were individually housed in Promethion behavioral phenotyping and respirometry cages (Sable Systems) with *ad libitum* access to food and water. Data on food and water consumption, distance travelled on the cage floor, VO₂ and VCO₂ were captured in real time via sensors and stored using the MetaScreen software (Sable Systems). Energy expenditure was determined by analyzing oxygen consumed and carbon dioxide exhaled and was corrected for lean mass. Respiratory quotient (RQ) was calculated based the ratio of oxygen consumed to carbon dioxide exhaled to determine the main fuel being used. For instance, RQ of 1 indicates carbohydrate usage as glucose uses six molecules of oxygen to generate six molecules of carbon dioxide. Food intake and water intake was measured in real time via sensors mounted in the food and liquid hoppers. Physical activity was measured by number of beam breakers in X, Y and Z axes. All data was analyzed in Rstudio, where relevant data were averaged over 12 hours to obtain day and night cycles as well as 24 hours to obtain daily measurements.

Mouse lean and fat mass were determined using the EchoMRI-900 (EchoMRI LCC) in a non-invasive manner. Mice were awake and un-anesthetized during all measurements. Measurements were taken before as well as after infection (day 9).

Oral glucose tolerance, insulin tolerance and pyruvate tolerance test

For glucose (GTT) and pyruvate (PTT) tolerance tests, mice fasted overnight were gavaged with a 30% glucose solution (1.5 g/kg body weight) and injected i.p. with pyruvate sodium solution (1 g/kg, Sigma Aldrich), respectively. For insulin tolerance test (ITT) mice were fasted for 4 hours and then injected i.p. with 0.75 U/kg of human fast working insulin (Actrapid). In all tests, blood glucose measurements were recorded at 0, 15, 30, 60 and 120 minutes using a glucometer (Libre).

Preparation of single cell suspensions from lung

Lung single cell suspensions were prepared using methods previously described.^{59,60} Briefly, lungs were incubated with 2 mg/mL of DNase I (Sigma Aldrich) and Collagenase IV (Sigma Aldrich) for 30 minutes. Lungs were dissociated and red blood cells were lysed using ACK lysis buffer (Thermo Fisher Scientific). Liver single cell suspensions were prepared using methods previously described.⁶⁰ Briefly, liver leukocytes were enriched using 35% isotonic Percoll (Cytiva, Marlborough). For adipose tissue single cell suspensions, BAT and epididymal WAT were collected in 5 mL of PBS and minced with scissors. Minced epididymal white adipose tissue and brown adipose tissue were digested in a 37°C water bath using 2 mg/mL of Collagenase II (Sigma Aldrich) for 25 minutes and 40 minutes, respectively. Digested tissues were filtered through a 100 μ m strainer and centrifuged at 500 g for 10 minutes. Supernatant was discarded and stromal vascular fraction (SVF) was resuspended in ACK lysis buffer. All single cell suspensions were washed with RPMI 1640 supplemented with 2% fetal calf serum (FCS) prior to being counted using trypan blue exclusion on a haemocytometer.

Flow cytometry

Cells (1×10^6) were washed with FACS wash (PBS supplemented with 2% FCS and 2mM EDTA) prior to being stained with PA-H2Db* conjugated to PE (NIH Tetramer Core Facility, Atlanta, GA, USA) for 1 hour at 4°C in FACS wash. After tetramer staining, cells were further stained with a surface receptor antibody cocktail containing FcBlock (2.4G2, BD Bioscience) and LIVE/DEAD fixable blue dead cell stain in FACS wash (Thermo Fisher Scientific) for 30 minutes at 4°C. For surface staining, cells were incubated for 30 minutes at 4°C with the following monoclonal antibodies: CD4 (RM4-5), CD8 (53-6.7) and CD44 (IM7).

For intracellular staining of cytokines, cells were stimulated with 1 $\mu\text{g/mL}$ of anti-CD3 ϵ mAb (clone 145-2C11, BD Bioscience) in RPMI 1640 supplemented with 10% FCS containing 1:1000 Golgi-plug (BD Biosciences) for 5 hours at 37°C. Following surface staining, the cells were fixed with 100 μL of Cytofix/Cytoperm (BD Bioscience) for 20 minutes at 4°C. Cells were incubated in 1x Permeabilization buffer for 1 hour at 4°C containing a cocktail of the following monoclonal antibodies: IFN- γ (XMG1.2) and TNF- α (MP6-XT22). Cells were washed in 1x Permeabilization buffer and resuspended in FACS wash buffer prior to acquisition. All flow cytometry acquisition was performed on BD Fortessa using FACSDiva software (BD Biosciences) and all analysis was performed using FlowJo10 (TreeStar).

Histological analysis

Paraffin-embedded brown adipose tissue collected from infected chow- and AIN93G-fed mice was sectioned at 5 μm and stained with hematoxylin and eosin (H&E). Slides were imaged by Leica Aperio XT slide scanner (Leica Biosystems) at x40 magnification and imported into ImageScope (Leica Biosystems). Individual fields (400 \times 300 μm) randomly selected from the scanned images were analyzed using QuPath (Queen's University, Belfast, Northern Ireland) or ImageJ (the National Institutes of Health, USA). Number of nuclei was determined in QuPath using the positive cell detection function. Lipid droplet diameter was determined in ImageJ by manual quantification and data points were imported into RStudio for graphic generation.

Cytokine quantification in plasma

For plasma samples, blood in EDTA-coated tubes was centrifuged at 2000 g for 15 minutes and plasma collected. The cytokine (IFN- α , IFN- β and IFN- γ) concentrations in plasma were quantified using the LEGENDplex kit (BioLegend). All kits were used according to the manufacturer's instructions.

Viral plaque assays

MDCK cells (4.5 \times 10⁵/well) were seeded into 6-well culture plates. Plates were incubated for 24 hours at 37°C, 5% CO₂. Lung lobes from infected mice were homogenized in PBS and centrifuged for 5 minutes at 2000 g to remove debris. Serially diluted lung homogenates in RPMI 1640 were added to the MDCK cells in 6-well culture plate (150 μL /well) and incubated at 37°C for 45 mins. The cells in each well were then overlaid with 3mL of L15 media (Sigma Aldrich) containing 1% (w/v) of Avicel (FMC biopolymer) and 1 $\mu\text{g/mL}$ of trypsin (Worthington Biochemicals). After further incubation at 37°C, 5% CO₂ for 3 days, the cells were washed with PBS, fixed with methanol and stained with crystal violet for visualization. Plaque forming units (PFU) was calculated as per lobe.

RNA preparation and qRT-PCR

Organs were preserved in RNAlater (Sigma Aldrich) and stored at -80°C . RNA extraction was performed using Trisure (Bioline) according to the manufacturer's instructions and RNA quantity determined using a NanoDrop (2000c, Thermo Fisher Scientific). Purified RNA was reversely transcribed using the Tetro cDNA synthesis Kit with random primers (Bioline).

Relative mRNA expression level was determined using the 2 $(-\Delta\Delta\text{C(T)})$ method and 18S as the reference gene. All quantitative reverse-transcriptase (qRT-PCR) was performed using SYBR NoROX master mix (Bioline) on a Roche LightCycler480. Primer sequences for each gene are described in [Table S3](#).

To determine viral nucleoprotein (NP) mRNA copy number, absolute viral NP quantification was performed as described.⁵⁹ Briefly, RNA was extracted from 1 \times 10⁷ IAV (PR8) and transcribed using viral nucleoprotein specific primers (IAV NP – forward CAGCC-TAATCAGACCAAATG; IAV NP – reverse TACCTGCTTCTCAGTCAAG). The cDNA product was subsequently purified and total copy number was determined based on size and yield of the product.

RNA sequencing

Mice fed on chow or AIN93G diets for 3wk *ad libitum* were infected with IAV. The hypothalamus, brown adipose tissue and liver were collected before and after infection at day 7 post infection in both diet-fed groups (n = 3–4). In total there were 47 samples which underwent RNA extraction using methods described above.

RNA was sequenced by the GENEWIZ Genomics Centre, China. Libraries were prepared using Illumina's TruSeq Stranded mRNA kit and sequencing was performed on an Illumina HiSeq 2000 platform as 150 base pair, paired end reads. Quality assessment and pre-processing of raw reads was performed by the Sydney Informatics Hub, University of Sydney. Briefly, the quality of the reads was assessed using FastQC (v 0.11.7) and MultiQC (v 1.5). Samples contained 30.3–42.7 million pairs of raw sequencing reads. Adaptors were trimmed using BBDuk (v 38.26). Trimmed sample FASTQ files were aligned as pairs to the mouse reference genome Mouse mm10 (GRCm38) using STAR (v 2.7.2b), GenBank Assembly ID: GCA_000001635.8 with default or recommended settings. Gene annotations (v 98) were obtained from Ensembl. Sequencing libraries were confirmed to be reverse strand-aware using RSeqQC's infer_experiment.py tool (v 2.6.4). STAR (v2.7.2b) generated the raw counts for differential expression analysis with DESeq2 ([Table S4](#)). Sample S-011 was removed as it was deemed an outlier.

Pre-processing was performed using published methods.⁶¹ Briefly, a count per million threshold equivalent to ~ 10 raw expression value was applied to remove all lowly expressed genes. Samples with total reads lower than two standard deviations from the tissue means were removed. Highly variable genes were queried from normalised log₂ expression values (log₂ (x+1) NC) of the filtered datasets. Filtered genes were annotated using org.Mm.eg.db.

Differential gene expression analysis was performed using DESeq2 with the following criteria: false discovery rate (FDR) < 0.05 and a \log_2 Fold Change > 1. Differential gene expression analysis was performed independently in each organ for the following pairwise comparisons: Infected chow versus uninfected chow, infected AIN93G versus uninfected AIN93G and infected AIN93G versus infected chow. Each pairwise comparison was used when indicated.

DEGs were submitted to the gene over-representation test (enrichGO) provided by ClusterProlifer. The minimal gene set size was set at three, and an FDR < 0.05 cut-off was set for significance. All GO enrichment results were semantically reduced using Simplify provided by ClusterProlifer with a cut-off threshold set at 0.5. Z-score was calculated by subtracting the number of DEGs with a positive fold change from the number of DEGs with a negative fold change. This number was then divided by the square root of the total number of DEGs in a pathway.

To evaluate genes involved in myogenesis and adipogenesis, we retrieved a list of genes belonging to myogenesis (GO:0007519) and adipogenesis (GO:0045444) GO terms from the mouse genome database (http://www.informatics.jax.org/vocab/gene_ontology). DEGs were matched against the myogenesis and adipogenesis gene lists. Top 5 upregulated and down regulated genes from each GO term were utilised.

QUANTIFICATION AND STATISTICAL ANALYSIS

Graphs were generated in RStudio or Prism 8 (GraphPad Software). All statistical analysis was performed in RStudio or Prism 8. The group differences in survival studies were determined using log-rank Mantel-Cox test. The pair-wise group differences were examined by Student's t-test or Mann-Whitney test. Differences between three or more groups were assessed by one-way ANOVA followed by post-hoc comparisons with Tukey's multiple test correction. Differences between three or more groups and two or more treatments was assessed by two-way ANOVA followed by post-hoc comparisons with Sidak's multiple test correction. Differences between two treatments across time-courses was determined by two-way repeated measures ANOVA. The level of significance was set at $p = 0.05$.

To determine whether the PFU and NP numbers are equivalent in the chow and AIN93G fed groups, we first performed power calculation to determine the smallest effect size of interest that our study had 90% power to detect. This information was then used to set standardised equivalence boundaries for a Welch two-sample equivalence t-test with the null hypothesis that viral loads differ between chow and AIN93G fed mice.

Supplemental information

**The quality of energy- and macronutrient-balanced
diets regulates host susceptibility
to influenza in mice**

Taylor A. Cootes, Nayan D. Bhattacharyya, Susie S.Y. Huang, Lina Daniel, Kim S. Bell-Anderson, Sebastian A. Stifter, Tracy Chew, Samantha M. Solon-Biet, Luis R. Saraiva, Yi Cai, Xinchun Chen, Stephen J. Simpson, and Carl G. Feng

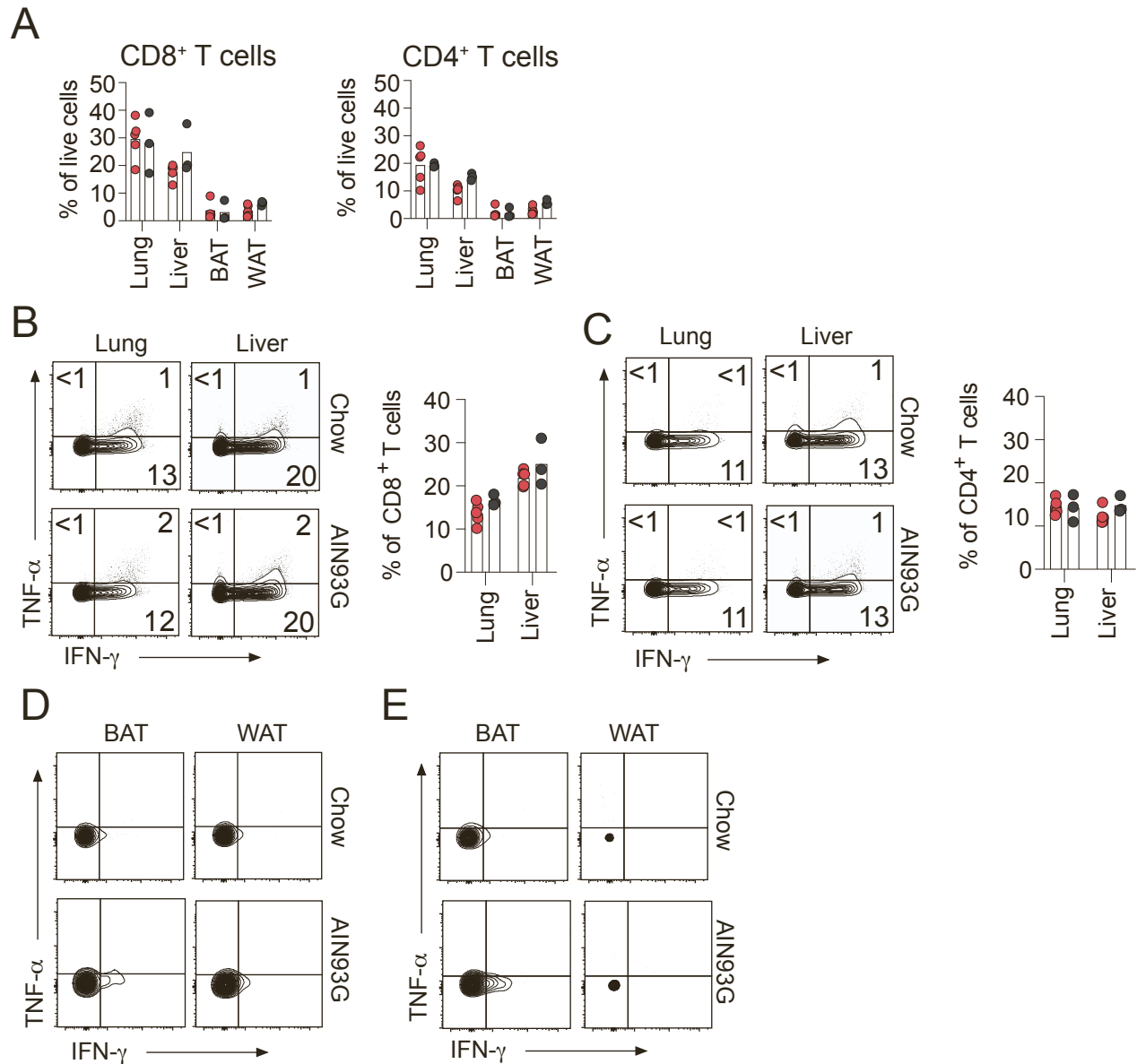


Figure S1. IFN- γ expression and production in non-lymphoid organs of IAV-infected chow and AIN93G fed mice. Mice ($n = 5$) fed with chow (red symbols) or AIN93G (black symbols) diets ad libitum for 3 wks were inoculated i.n. with 5 PFU IAV and various tissues harvested at day 9 p.i. **(A)** Percentage of CD4⁺ and CD8⁺ T cells in total live cells in the lung, liver, BAT and WAT determined by flow cytometry. Symbols represent individual mice, and bars denote group mean. **(B - E)** Single cell suspension prepared from the various tissues of infected mice were stimulated with soluble anti-CD3 mAb for 5 hours ex vivo before intracellular cytokine staining. Representative flow cytometry plots (left) and summary data (right) of the percentage of IFN- γ producing **(B)** CD8⁺ and **(C)** CD4⁺ T cells in lung and liver. Representative flow cytometry plots showing intracellular cytokine staining in **(D)** CD8⁺ and **(E)** CD4⁺ T cells in BAT and WAT.

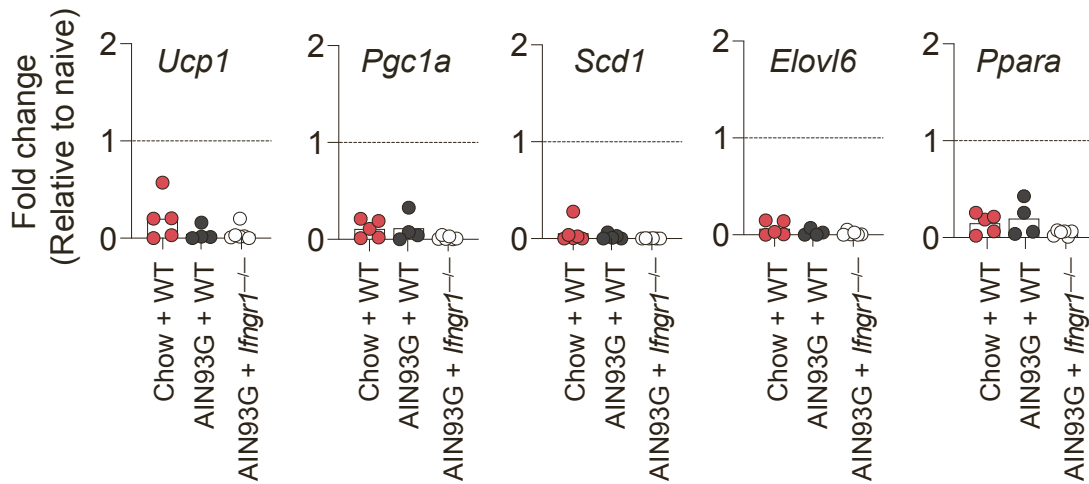


Figure S2. IAV infection downregulates thermogenic genes in the BAT irrespective of diet regime or presence of IFN- γ signalling. WT and *Ifngr1*^{-/-} mice (n = 4 – 5) fed with chow or AIN93G diets ad libitum for 3 weeks were infected with 2.5 PFU IAV i.n.. Data shown are fold change in mRNA expression in the BAT of the infected mice over naïve chow-fed mice as measured by qRT-PCR at day 9 p.i. Symbols represent individual mice and bars denote group mean. Dotted lines indicate the gene expression levels of naïve chow-fed mice.

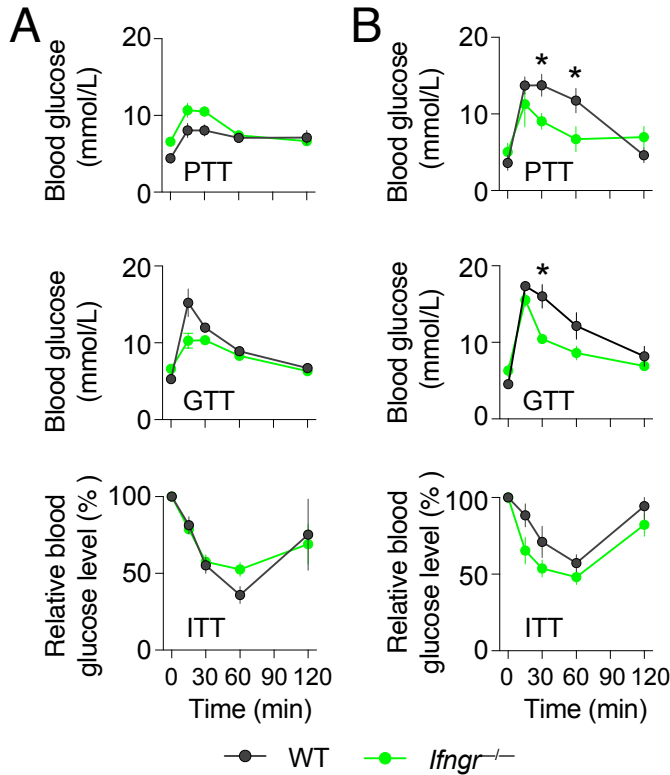


Figure S3. IFN- γ modulates glucose metabolism in IAV-infected AIN93G-fed mice. WT and *Ifngr*^{-/-} mice (n = 5) fed with AIN93G diets for 3 wks were infected with 2.5 PFU IAV i.n.. PTT, GTT, ITT were performed **(A)** before and **(B)** 9 days after IAV infection. Data shown are mean blood glucose levels \pm SD determined in PTT and GTT, or mean percentage \pm SD of baseline glucose levels measured at time 0 in ITT. Statistical analysis was performed using two-way repeated-measures ANOVA. *p < 0.05.

Table S3: List of qRT-PCR primer sequences. Related to STAR Methods

Gene	Forward (5')	Reverse (3')
18S	GTAACCCGTTGAACCCCAT	CCATCCAATCGGTAGTAGCG
Elovl6	TCAGCAAAGCACCCGAAC	AGCGACCATGTCTTTGTAGGAG
IAV NP	CAGCCTAATCAGACCAAATG	TACCTGCTTCTCAGTTCAAG
Ifna	TGCAACCCTCCTAGACTCATT	CCAGCAGGGCGTCTTCCT
Ifnb	ATGAGTGGTGGTTGCAGGC	TGACCTTTCAAATGCAGTAGA
Ifng	ACAATGAACGCTACACACTGCAT	TGGCAGTAACAGCCAGAAACA
Il1b	CAACCAACAAGTGATATTCTCCATG	GATCCACACTCTCCAGCTGCA
Nos2	CAGCTGGGCTGTACAAACCTT	CATTGGAAGTGAAGCGTTTCG
Pgc1a	GGACATGTGCAGCCAAGACTCT	CACTTCAATCCACCCAGAAAGCT
Ppara	TATGGAGTGACATAGAGTGTGCT	CCACTTCAATCCACCCAGAAAG
Scd1	TTCTTGCGATACACTCTGGTGC	CGGGATTGAATGTTCTTGTCG
Tnfa	AATGGCCTCCCTCTCATCAGTT	CCACTTGGTGGTTTGCTACGA
Ucp1	GTGAAGGTCAGAATGCAAGC	GGCAGTTGCCTAGTGAAAGGT